

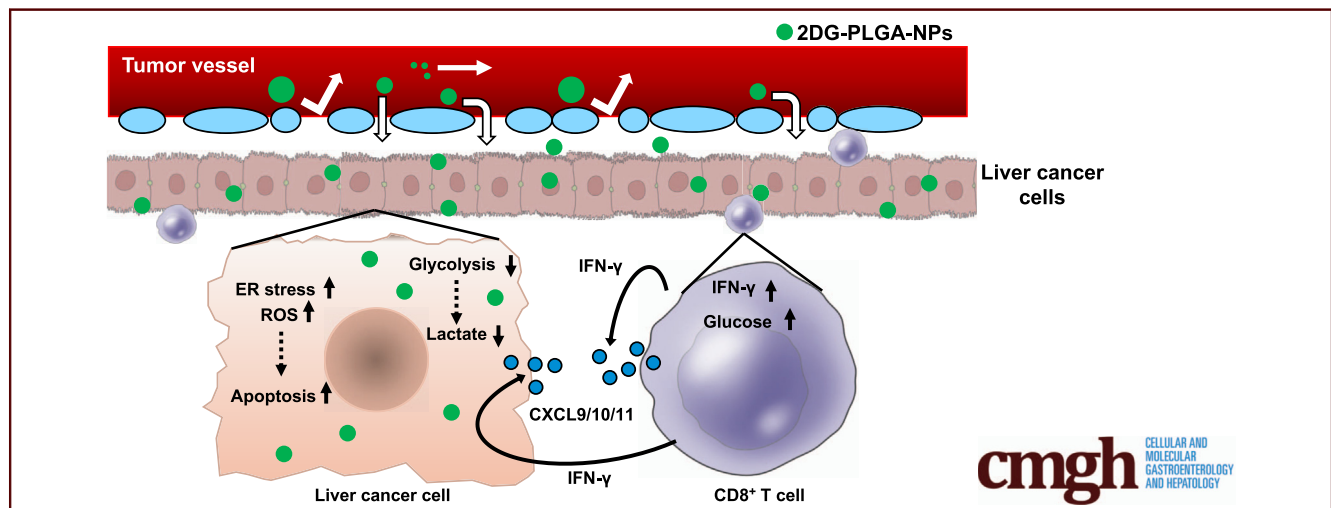
ORIGINAL RESEARCH

Nanoparticle-Mediated Delivery of 2-Deoxy-D-Glucose Induces Antitumor Immunity and Cytotoxicity in Liver Tumors in Mice



Kyo Sasaki,¹ Sohji Nishina,¹ Akira Yamauchi,² Kotaro Fukuda,⁴ Yuichi Hara,¹ Masahiro Yamamura,³ Kensuke Egashira,^{4,5} and Keisuke Hino¹

¹Department of Hepatology and Pancreatology, ²Department of Biochemistry, ³Department of Clinical Oncology, Kawasaki Medical School, Kurashiki, Japan; ⁴Sentan Pharma, Inc, Japan; ⁵Department of Translational Medicine, Kyushu University Graduate School of Medicine, Fukuoka, Japan



SUMMARY

The encapsulated 2-deoxy-D-glucose in poly(lactic-co-glycolic acid) nanoparticles showed antitumor immunity and cytotoxicity in liver tumors in mice. These 2-deoxy-D-glucose in poly(lactic-co-glycolic acid) nanoparticles not only amplified antitumor effects induced by sorafenib or anti-programmed death-1 antibody, but also suppressed anti-programmed death-1-resistant tumors.

BACKGROUND & AIMS: Immune checkpoint inhibitors have shed light on the importance of antitumor immunity as a therapeutic strategy for hepatocellular carcinoma (HCC). The altered glucose metabolism known as the Warburg effect recently has gained attention as a cancer immune-resistance mechanism. Considering glycolysis inhibitors as therapeutic agents, their specific delivery to cancer cells is critical not to induce adverse effects. Thus, we investigated antitumor effects of a glycolysis inhibitor, consisting of 2-deoxy-D-glucose (2DG)-encapsulated poly(lactic-co-glycolic acid) (PLGA) nanoparticles (2DG-PLGA-NPs), against hepatocellular carcinoma in mice.

METHODS: The antitumor effects of 2DG-PLGA-NPs were examined using hepatoma cell lines, xenograft tumors, and hepatocarcinogenic and syngeneic mouse models.

RESULTS: The 2DG-PLGA-NPs induced cytotoxic effects and antitumor immunity through enhanced T-cell trafficking. In

addition, 2DG-PLGA-NPs induced decreased lactate production and increased interferon- γ -positive T cells in liver tumors. Human CD8⁺ T cells cocultured with 2DG-PLGA-NP-treated Huh7 cells showed their increased interferon- γ production and glucose uptake compared with the CD8⁺ T cells co-cultured with PLGA-NP-treated Huh7 cells. Chemotaxis of CD8⁺ T cells was suppressed by lactate and enhanced by glucose. Interferon- γ enhanced CD8⁺ T-cell chemotaxis in both an autocrine and paracrine manner. Notably, the 2DG-PLGA-NPs augmented chemokine (CXCL9/CXCL10) production in liver tumors via interferon- γ -Janus kinase-signal transducers and activator of transcription pathway and 5' adenosine monophosphate-activated protein kinase-mediated suppression of histone H3 lysine 27 trimethylation. These 2DG-PLGA-NPs not only amplified antitumor effects induced by sorafenib or an anti-programmed death-1 antibody, but also suppressed anti-programmed death-1-resistant tumors.

CONCLUSIONS: The newly developed 2DG-PLGA-NPs showed antitumor immunity and cytotoxicity in liver tumors in mice, suggesting the potential of 2DG-PLGA-NPs for future clinical applications. (*Cell Mol Gastroenterol Hepatol* 2021;11:739-762; <https://doi.org/10.1016/j.jcmgh.2020.10.010>)

Keywords: PLGA; IFN- γ ; Lactate; Chemokine; Programmed Death 1.

Hepatocellular carcinoma (HCC) is the third leading cause of cancer-related death in the world. A recent study from the United States found that the incidence rate of HCC is continuously increasing in subgroups such as men aged from 55 to 64 years, and especially those born during the peak era of hepatitis C virus infection.¹ Patients with advanced HCC, including macrovascular invasion or extrahepatic spread, face a poor prognosis, with an expected median survival period of 6–8 months or 25% at 1 year.² Although multityrosine kinase inhibitors such as sorafenib and lenvatinib have prolonged the overall survival of patients with advanced HCC in the past decade,^{3,4} their therapeutic effects still are not satisfactory. Therefore, it is worth investigating new therapeutic agents that have antitumor effects in patients with advanced HCC.

Many reports have described various metabolic changes that enable cancer cells to survive,⁵ suggesting that metabolic pathways might be good targets for cancer therapy. In particular, cancer cells are characterized by altered glucose metabolism, known as the Warburg effect,⁶ in which a substantial amount of pyruvate is reduced to lactic acid instead of being directed into mitochondria. The Warburg effect recently has gained attention as a cancer immune-resistance mechanism.^{7,8} Concurrently, immune checkpoint inhibitors have shed light on the importance of antitumor immunity as a therapeutic strategy for HCC.^{9,10} Therefore, targeting glucose metabolism may be a promising approach for the development of new therapeutic agents for advanced HCC. The first step in glycolysis, the phosphorylation of glucose to form glucose-6-phosphate, is controlled by hexokinase. 2-Deoxy-D-glucose (2DG), a glucose analog, inhibits hexokinase, resulting in glycolytic inhibition, and has been reported to have cytotoxic effects against tumors in phase I/II clinical trials.^{11,12} However, 2DG does not seem to have a significant effect on tumor growth at a dose that does not induce serious adverse effects.^{11,12} These results suggest a need to develop an efficient drug delivery system for 2DG.

Tumor vessels have poorly aligned defective endothelial cells with wide fenestrae and lack a smooth muscle layer.¹³ Tumor tissue usually lacks lymphatic drainage. These characteristics are referred to as the *enhanced permeability and retention* effect.^{14–16} Molecules of certain sizes, such as nanoparticles, tend to accumulate in tumor tissue compared with their retention in normal tissue owing to the enhanced permeability and retention effect. Poly(lactic-co-glycolic acid) (PLGA), which is used for specific applications and has been approved by the Food and Drug Administration, is one of the most successfully developed biodegradable polymers used to formulate nanoparticles.¹⁷ Therefore, we encapsulated 2DG in PLGA nanoparticles (2DG-PLGA-NPs) to increase the efficiency of 2DG delivery to liver tumors. Here, we investigated whether 2DG-PLGA-NPs have antitumor effects, especially antitumor immunity, against HCC in mice, and elucidate the underlying mechanisms and their potential for clinical application.

Results

Physical Properties of 2DG-, Indocyanine Green-, and Fluorescein


Isothiocyanate-Encapsulated PLGA-NPs

Monodispersity of PLGA-NPs, 2DG-PLGA-NPs, indocyanine green (ICG)-PLGA-NPs, and fluorescein isothiocyanate (FITC)-NPs are shown in Figure 1A. The mean particle size distribution of each PLGA-NPs had a single peak, and the D₅₀ of the PLGA-NPs, 2DG-PLGA-NPs, ICG-PLGA-NPs, and FITC-PLGA-NPs were 172 nm, 120 nm, 205 nm, and 252 nm, respectively (Figure 1A, right panels). Transmission electron microscopy also showed the spherical nanoparticles with almost the same size in these PLGA-NPs (Figure 1A, left panels). The surface charge (zeta potential) was –10.3 mV for PLGA-NPs, –16.4 mV for 2DG-PLGA-NPs, –35.1 mV for ICG-PLGA-NPs, and –16.3 mV for FITC-PLGA-NPs. The zeta potential of 2DG-PLGA-NPs in the present study was similar to that of docetaxel-loaded PLGA-NPs (–18.6 mV) in a previous study.¹⁸ The loading capacity of these hydrophilic compounds was 8.1% ± 0.4% for 2DG-PLGA-NPs, 6.8% ± 0.6% for ICG-PLGA-NPs, and 6.8% ± 0.4% for FITC-PLGA-NPs.

In Vivo Delivery of Nanoparticles in Nude Mice With Xenograft Liver Tumors

We assessed in vivo distribution of ICG accumulation in the nude mice until 10 days after injection of ICG-PLGA-NPs. ICG gradually and specifically accumulated in the xenograft liver tumors in the 10 days after injection of the ICG-PLGA-NPs, and the relative optical signal intensity of ICG in the tumors gradually increased through day 7 (Figure 1B). However, we need to pay attention in interpreting these results because superficial organs (tumors) dominate the analysis when fluorescence reflectance imaging is used. We also investigated whether FITC-PLGA-NPs were delivered to the tumor cells in the xenograft tumors. Green puncta around the nucleus, possibly in the cytoplasm were observed in the same manner both 3 days and 7 days after the injection of the FITC-PLGA-NPs (Figure 1C).

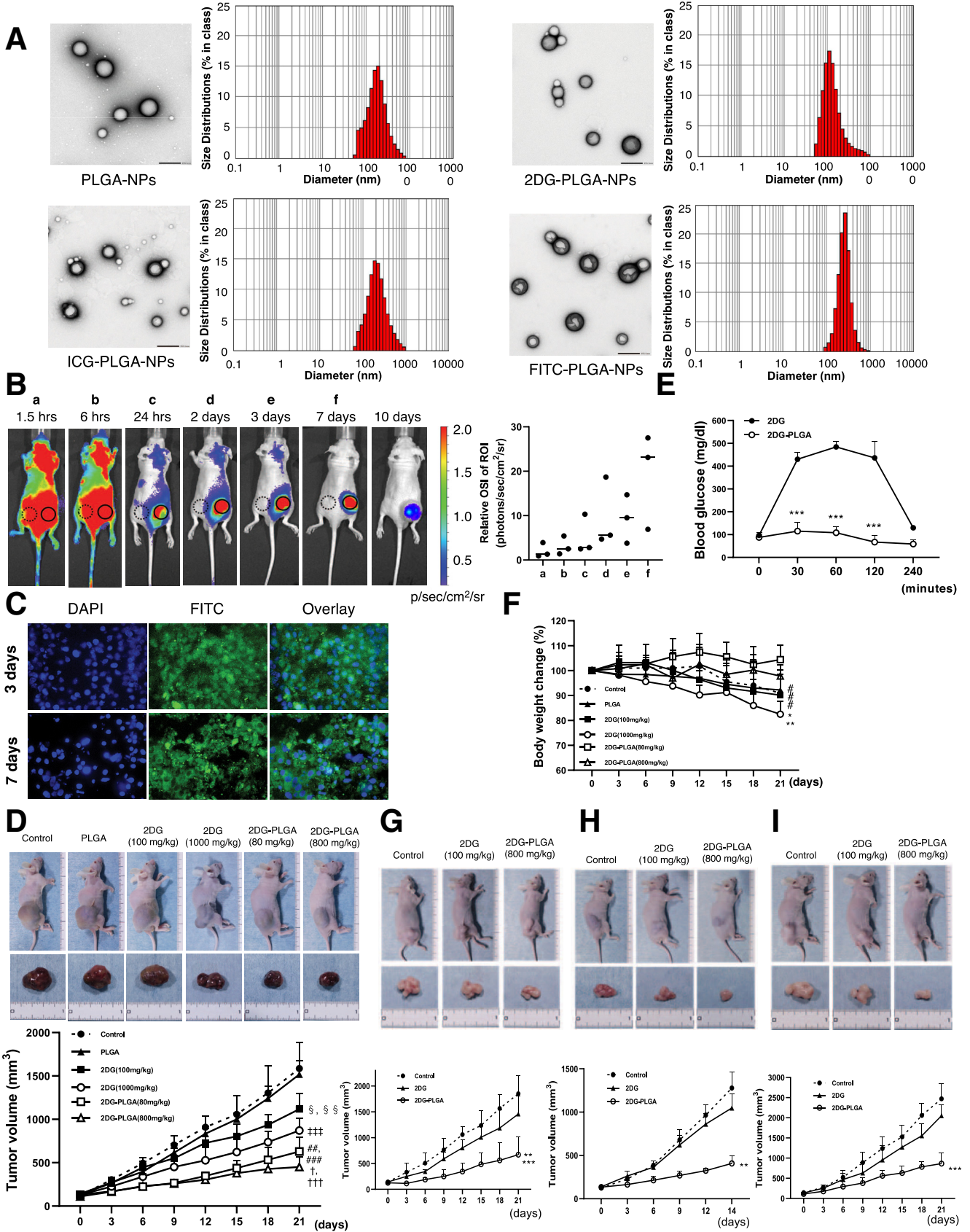
Abbreviations used in this paper: 2DG, 2-Deoxy-D-glucose; 2-NDBG, 2-(N-[nitrobenz-2-oxa1,3-diazol-4-yl]amino)-2-deoxyglucose; AMPK, AMP-activated protein kinase; ATP, adenosine triphosphate; CCL, C-C motif chemokine; CCR, C-C chemokine receptor type 4; DAPI, 4',6-diamidino-2-phenylindole; DEN, diethylnitrosamine; GSH, glutathione; ER, endoplasmic reticulum; EZH2, enhancer of zeste homologue 2; FBS, fetal bovine serum; ¹⁸F-FDG, ¹⁸F-2-fluoro-2-deoxyglucose; FITC, fluorescein isothiocyanate; H3K27me3, H3 lysine 27 trimethylation; HCC, hepatocellular carcinoma; ICG, indocyanine green; IFN- γ , interferon- γ ; JAK, Janus kinase; mRNA, messenger RNA; mTOR, mammalian target of rapamycin; NP, nanoparticles; PD1, programmed death 1; PD-L1, programmed death-ligand 1; PLGA, poly(lactic-co-glycolic acid); ROS, reactive oxygen species; STAM, stelic animal model; STAT, signal transducers and activator of transcription; homologue, 2; TNF- α , tumor necrosis factor- α ; Treg, regulatory T cell.

 Most current article

© 2020 The Authors. Published by Elsevier Inc. on behalf of the AGA Institute. This is an open access article under the CC BY-NC-ND license (<http://creativecommons.org/licenses/by-nc-nd/4.0/>).

2352-345X

<https://doi.org/10.1016/j.jcmgh.2020.10.010>



Cytotoxic Effect of 2DG-PLGA-NPs in Nude Mice With Xenograft Tumors

Treatment with 2DG-PLGA-NPs resulted in a significant growth reduction of the xenograft liver tumors (Figure 1D). The blood glucose levels were increased by as much to 500 mg/dL at 1 hour after 2DG administration, but remained within the normal range for 4 hours after 2DG-PLGA-NP administration in mice that had been treated for 14 days (Figure 1E). Body weight also was decreased significantly in the mice treated with 2DG (1000 mg/kg) compared with mice treated with 2DG-PLGA-NPs (Figure 1F). These results suggest that replacement of 2DG administration with 2DG-PLGA-NPs reduced the 2DG-induced adverse effects. Treatment with 2DG-PLGA-NPs resulted in a significant growth reduction in the xenograft colon tumors (Figure 1G), xenograft renal tumors (Figure 1H), and xenograft pancreatic tumors (Figure 1I), indicating the potential antitumor effects of this method against various tumors.

Treatment with 2DG resulted in the suppression of total and glycolytic adenosine triphosphate (ATP) production, but not mitochondrial oxidative ATP production in the Huh7 cells (Figure 2A), in agreement with no effects on the mitochondrial oxygen consumption ratio (Figure 2B). Treatment with 2DG-PLGA-NPs resulted in the augmentation of AMP-activated protein kinase (AMPK) phosphorylation and the expression of endoplasmic reticulum (ER) stress-related chaperones, and the attenuation of mammalian target of rapamycin (mTOR) activity and its downstream molecules such as S6, Rb, cyclin D1, proliferating cell nuclear antigen, and vascular endothelial growth factor-A,^{19–22} in xenograft liver tumors (Figure 2C). Treatment with 2DG-PLGA-NPs decreased CD34-positive vessel density (Figure 2D) and increased reactive oxygen species (ROS) production (Figure 2E) in xenograft liver tumors. We confirmed that 2DG showed an increase in the frequency of cells in the G0/G1 phase and a decrease in the frequency of those in the S/G2/M phase (Figure 3A), and reduced

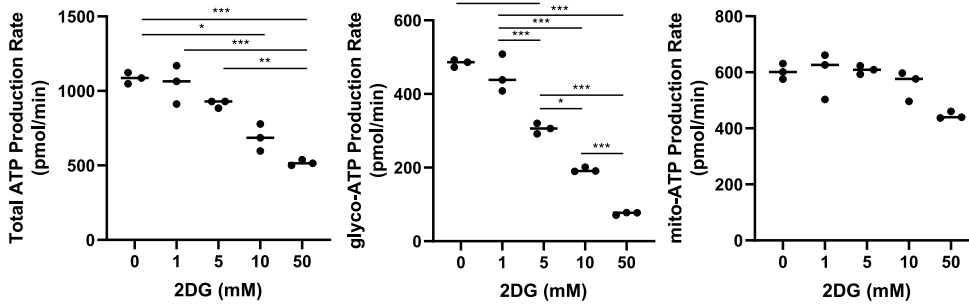
glutathione (GSH) production in the Huh7 cells and HepG2 cells (Figure 3B). Thus, treatment with 2DG-PLGA-NPs resulted in an increase in terminal deoxynucleotidyl transferase-mediated deoxyuridine triphosphate nick-end labeling-positive cells and cleaved caspase 3-positive cells in xenograft liver tumors (Figure 3C and D), suggesting the facilitation of apoptosis by the 2DG-PLGA-NPs. ER stress also contributed to 2DG-induced apoptosis because inhibition of tumor growth by 2DG was suppressed by treatment with 4-phenylbutyric acid, an ER stress inhibitor (Figure 3E). These results suggested that the cytotoxic effect of 2DG is realized via oxidative stress, ER stress, and inactivation of mTOR in vivo, as described previously.²³

Antitumor Effects of 2DG-PLGA-NPs in Immunocompetent Mice

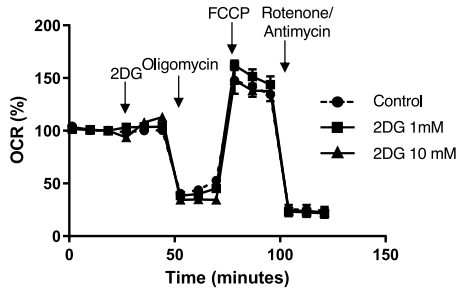
To explore antitumor effects, including those on antitumor immunity, we used an immunocompetent stelic animal model (STAM) mouse and diethylnitrosamine (DEN)-induced HCC mouse model. STAM mice and DEN-treated mice presented with multiple large tumors in the liver at 16 weeks and 9 months of age, respectively (Figure 4A and B). Treatment with 2DG-PLGA-NP (800 mg/kg) significantly suppressed tumor growth in STAM mice (Figure 4A) and DEN-treated mice (Figure 4B) compared with no treatment (control), but 2DG treatment alone did not, except for tumor number in STAM mice. We confirmed the accumulation of ICG in the liver tumors of 9-month-old male DEN-treated mice 7 days after injection of ICG-PLGA-NPs, using an in vivo imaging system (Figure 4C). In addition, FITC accumulated around the nucleus, possibly in the cytoplasm, in tumor tissue, but was colocalized mainly with Kupffer cells in nontumor tissue 5 days after injection of FITC-PLGA-NPs in a STAM mouse (Figure 4D). The relative tumor volume with respect to that of the control (no treatment) was decreased significantly by 2DG-PLGA-NP (80 mg/kg) treatment in

Figure 1. (See previous page). Physical properties of nanoparticles, in vivo accumulation of ICG-PLGA-NPs and FITC-PLGA-NPs, and the antitumor effects of 2DG-PLGA-NPs in nude mice. (A) PLGA-based nanoparticles (PLGA-NPs, 2DG-PLGA-NPs, ICG-PLGA-NPs, and FITC-PLGA-NPs) in transmission electron microscopy (left panels), and a histogram representing the nanoparticle diameter distribution of PLGA-NPs, 2DG-PLGA-NPs, ICG-PLGA-NPs, and FITC-PLGA-NPs (right panels). Transmission electron microscopy: scale bar: 200 nm. (B) In vivo distribution of accumulated ICG after ICG-PLGA-NP injection in 3 nude mice bearing Huh7 cell xenograft tumors, as observed using in vivo imaging system. The relative optical signal intensity (OSI) of the region of interest (ROI) represents the ratio of the ROI (solid circle) intensity in the xenograft tumors to that (dotted circle) in the nontumorous regions. (C) FITC accumulation in the xenograft tumor cells 3 and 7 days after the FITC-PLGA-NP injection. DAPI stains the nucleus. (D) Huh7 xenograft tumors and growth curves of the mice 21 days after the commencement of treatment, 6 groups (n = 5 for each group). Administration frequency was weekly for PLGA and 2DG-PLGA-NPs (intravenous administration), and daily for 2DG (intraperitoneal administration). ^{†††}P < .001 vs the control, PLGA, and 2DG (100 mg/kg); ^{†††}P < .001, [†]P < .05 vs 2DG (1000 mg/kg). ^{###}P < .001 vs control and PLGA, ^{##}P < .01 vs 2DG (100 mg/kg); [‡]P < .001 vs control and PLGA; ^{§§}P < .01 vs control, and [§]P < .05 vs PLGA. (E) Blood glucose levels up to 4 hours after intraperitoneal 2DG (1000 mg/kg) or intravenous 2DG-PLGA-NP (800 mg/kg) injection in the nude mice, which had been treated for 14 days. ^{***}P < .001. (F) Body weight changes in the nude mice shown in panel D. ^{***}P < .001 vs 2DG-PLGA-NP (80 mg/kg), ^{*}P < .05 vs 2DG-PLGA-NP (800 mg/kg); and [#]P < .05 control, PLGA or 2DG (100 mg/kg) vs 2DG-PLGA-NP (80 mg/kg). (G) HT29 cell xenograft colon tumors and growth curves of the mice at 21 days after the commencement of treatment in 3 groups (control, 2DG [100 mg/kg], and 2DG-PLGA-NPs [800 mg/kg]) (n = 5 for each group). Administration frequency was daily for 2DG (intraperitoneal) and weekly for 2DG-PLGA-NPs (intravenous). ^{**}P < .01 vs 2DG, ^{***}P < .001 vs the control. (H) OS-RC-2 cell xenograft renal tumors and growth curves of the mice 14 days after the commencement of treatment in the same groups as indicated in panel G. ^{**}P < .01 vs the control and 2DG. (I) BxPC3 cell xenograft pancreatic tumors and growth curves in the mice 21 days after the commencement of treatment in the same groups as indicated in panel G. ^{***}P < .001 vs the control and 2DG.

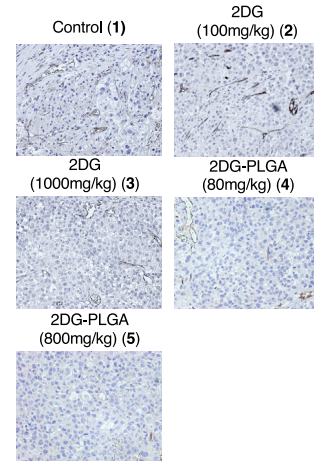
A



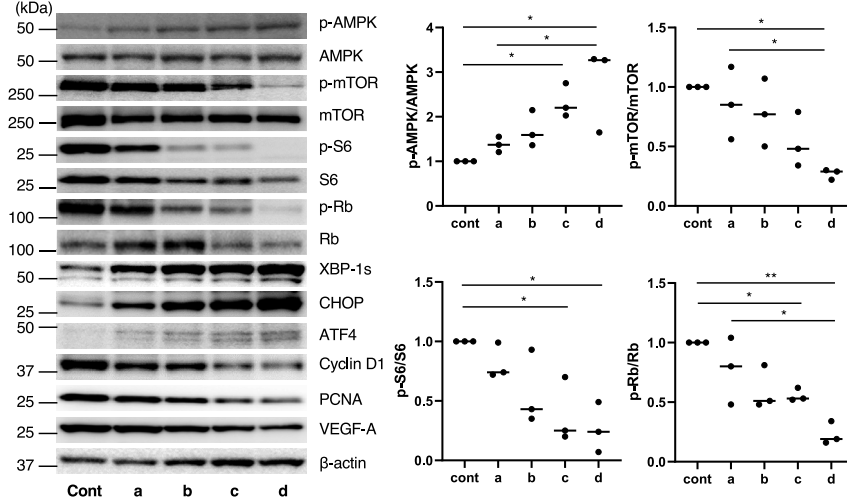
B



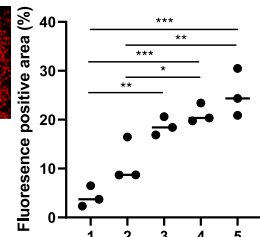
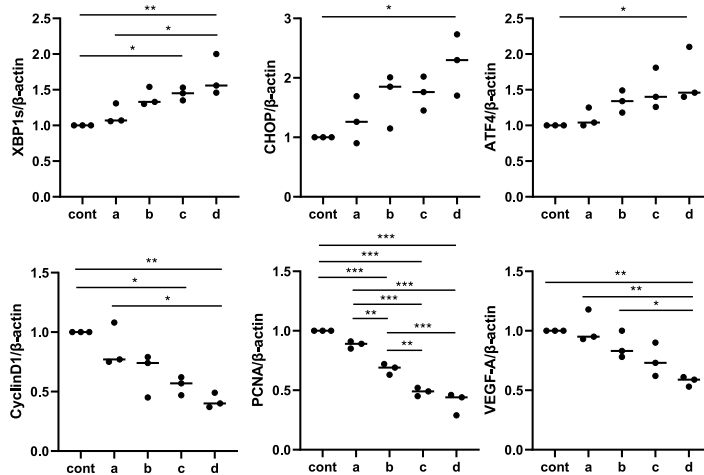
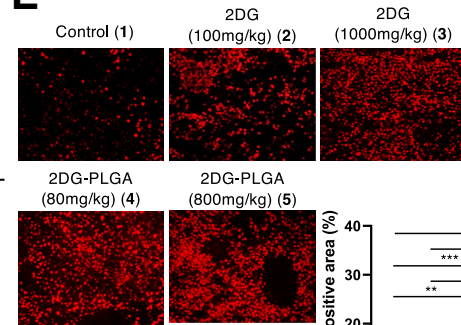
D



C



E



STAM mice, but not in nude mice (Figure 4E). We found a liver tumor with infiltrated mononuclear cells in a STAM mouse treated with 2DG-PLGA-NPs, but not in a mouse treated with PLGA-NPs alone (Figure 4F). The STAM mice treated with 2DG-PLGA-NPs showed a significantly greater number of infiltrated CD3-positive cells than did those without treatment, but those treated with 2DG alone did not (Figure 4G). No mice presented with Foxp3-positive regulatory T cell (Treg) infiltration (Figure 4H). These results suggest that the greater antitumor effect in the STAM mice potentially resulted from the antitumor immunity induced by the 2DG-PLGA-NPs.

Mechanisms by Which 2DG-PLGA-NPs Enhance the Messenger RNA Level of Chemokines

Treatment with 2DG-PLGA-NPs resulted in a significant increase in *Cxcl9/Cxcl10/Cxcl11* messenger RNA (mRNA) levels in the liver tumors of STAM mice (Figure 5A). CXCL9/CXCL10/CXCL11 are known to be induced by interferon- γ (IFN- γ).²⁴ STAM mice treated with 2DG-PLGA-NPs showed a significantly greater number of IFN- γ -positive mononuclear cells in their liver tumors than did the untreated mice (Figure 5B). IFN- γ has been shown to activate transcription of CXCL9/CXCL10/CXCL11 via Janus kinase (JAK)-signal transducers and activator of transcription (STAT) 1 signaling.²⁵ Treatment with 2DG-PLGA-NPs resulted in the significantly up-regulated phosphorylation of JAK1/2 and STAT1 in the STAM mice compared with that in the mice treated with PLGA alone (Figure 5C). Thus, the treatment with 2DG-PLGA-NPs increased the mRNA level of *Cxcl9/Cxcl10/Cxcl11* through the IFN- γ -JAK-STAT1 pathway in liver tumors.

Treatment with 2DG resulted in an increase in the production of CXCL9/CXCL10/CXCL11 in a dose-dependent manner in the presence of IFN- γ and tumor necrosis factor- α (TNF- α) in the Huh7 cells (Figure 5D) and HepG2 cells (Figure 5E), suggesting a possible alternative IFN- γ -independent pathway through which 2DG increases chemokine production. In this regard, histone methyltransferase, enhancer of zeste homologue 2 (EZH2)-mediated histone H3 lysine 27 trimethylation (H3K27me3), has been

reported to repress the tumor production of CXCL9/CXCL10.²⁶ It also has been reported that AMPK phosphorylates EZH2 to disrupt the interaction between EZH2 and suppressor of zeste 12, another core component of the polycomb repressive complex 2, leading to attenuated polycomb repressive complex 2-dependent methylation of H3K27me3 modification.²⁷ These observations suggest that AMPK activation potentially activates the production of tumor-inducing CXCL9/CXCL10 through the attenuation of H3K27me3 modification. Treatment with 2DG-PLGA-NPs resulted in the activation of AMPK and EZH2 through their phosphorylation (Figure 5F) and the reduced expression of H3K27me3 (Figure 5G) in the liver tumors of STAM mice. Treatment with the AMPK inhibitor compound C abrogated the 2DG-induced activation of AMPK by phosphorylation and reduction of the H3K27me3 level in Huh7 cells (Figure 5H). Finally, treatment with compound C blunted the augmented production of CXCL9/CXCL10 mRNA induced by 2DG, but not the CXCL11 mRNA (Figure 5I). These results suggest that the 2DG-PLGA-NPs enhanced the production of CXCL9/CXCL10 through the AMPK-EZH2-H3K27me3 pathway.

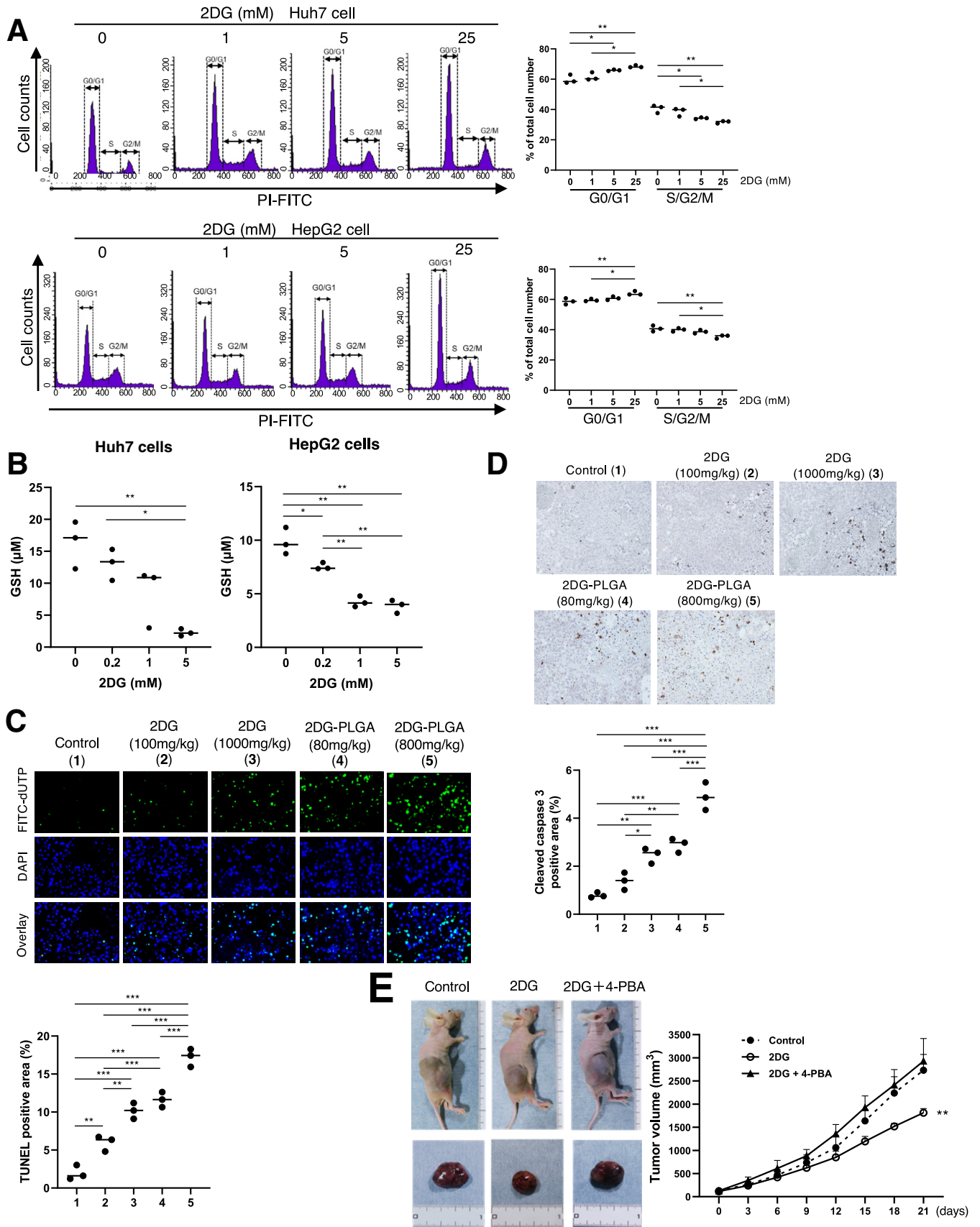
Defective T-Cell Trafficking Abrogates the Antitumor Effects of 2DG-PLGA-NPs

T-cell accumulation in tumor tissue has been shown to be dependent on the chemokine receptor CXCR3,²⁸ which binds to the structurally and functionally related chemokines CXCL9/CXCL10/CXCL11. The administration of anti-CXCR3 (Figure 6A) abrogated the reduction in liver tumor growth (tumor maximum diameter and tumor volume) induced by the 2DG-PLGA-NPs (Figure 6B) and abolished T-cell accumulation in liver tumors (Figure 6C) in DEN-treated mice at 9 months of age. These results suggest that the antitumor effects of 2DG-PLGA-NPs are dependent on T-cell migration into tumor tissue.

CD8⁺ T-Cell Migration Is Directly Dependent on Lactate, IFN- γ , and Glucose

Genetically engineered tumors with reduced lactate production have shown increased infiltration with

Figure 2. (See previous page). Effects of 2DG or 2DG-PLGA-NPs on ATP production, cytotoxicity, tumor vessel formation, and ROS production. (A and B) Total, glycolytic, and mitochondrial ATP production rates were measured in the Huh7 cells (3×10^4 cells/well) using a Seahorse XF24 Extracellular Flux Analyzer. The extracellular acidification rate and oxygen consumption rate (OCR) were analyzed after injection of 2DG (0, 1, 5, 10, and 50 mmol/L). Glycolytic and mitochondrial ATP production rates were determined based on the extracellular acidification rates and OCRs using an Agilent Seahorse XFp Real-Time ATP rate assay report generator. * $P < .05$, ** $P < .01$, and *** $P < .001$. (C) Immunoblots showing results for p-AMPK, AMPK, p-mTOR, mTOR, p-S6, S6, p-Rb, Rb, spliced x-box binding protein 1 (XBP-1s), CCAAT/enhancer binding protein-homologous protein (CHOP), activating transcription factor 4 (ATF4), cyclin D1, proliferating cell nuclear antigen (PCNA), and vascular endothelial growth factor (VEGF)-A, performed using xenograft tumors in each nude mouse group ($n = 3$). Column a, 2DG (100 mg/kg); column b, 2DG (1000 mg/kg); column c, 2DG-PLGA-NP (80 mg/kg); and column d, 2DG-PLGA-NP (800 mg/kg). Administration frequency was daily for 2DG (intraperitoneal) and weekly for 2DG-PLGA-NPs (intravenous). The amount of phosphorylated protein was normalized to total protein. The amount of some proteins was normalized to that of β -actin. * $P < .05$, ** $P < .01$, and *** $P < .001$. (D) Immunostained CD34-positive vessels and (E) dihydroethidium staining for detecting ROS production in the Huh7 cell xenograft tumors 21 days after the commencement of treatment in the 5 groups as indicated ($n = 3$ for each group) (original magnification: $\times 400$). Administration frequency was daily for 2DG (intraperitoneal) and weekly for 2DG-PLGA-NPs (intravenous). National Institutes of Health image analysis software was used to quantify the mean percentage of the positively stained area of 5 randomly selected fields in the digital images of each tumor. * $P < .05$, ** $P < .01$, and *** $P < .001$. Column 1, control; column 2, 2DG (100 mg/kg); column 3, 2DG (1000 mg/kg); column 4, 2DG-PLGA-NP (80 mg/kg); and column 5, 2DG-PLGA-NP (800 mg/kg). Cont, control; FCCP, carbonyl cyanide 4-(trifluoromethoxy) phenylhydrazone.



IFN- γ -producing T and natural killer cells in immunocompetent C57BL/6 mice.⁷ The ex vivo experiments showed that the lactate production was significantly lower in the 2DG-PLGA-NP-treated Huh7 cells than in the PLGA-NP-treated Huh7 cells (Figure 6D and E) and that IFN- γ production was significantly greater in the CD8⁺ T cells cocultured with 2DG-PLGA-NP-treated Huh7 cells than it was in the CD8⁺ T cells co-cultured with the PLGA-NP-treated Huh7 cells (Figure 6D and F). EZ-TAXIScan (Effector Cell Institute, Tokyo, Japan), a real-time, cell mobility analysis device, showed that lactate (Figure 7A, lanes 1 and 2) and a low pH (Figure 7A, lanes 1 and 3) significantly inhibited the mobility of the CD8⁺ T cells in the presence of CXCL10, respectively.

Interestingly, CD8⁺ T cells showed enhanced mobility in the presence of the culture supernatant of the CD8⁺ T cells incubated with IFN- γ (Figure 7B, lanes 1 and 2), which was suppressed by the addition of anti-CXCR3 (Figure 7B, lanes 2 and 3). Treatment with IFN- γ resulted in significantly increased production of *CXCL9/CXCL10/CXCL11* mRNA in the CD8⁺ T cells (Figure 7C). Indeed, these results suggest an autocrine role for IFN- γ in the chemokine production of CD8⁺ T cells, and were consistent with previous observations indicating that IFN- γ derived from CD8⁺ T cells directly enhances their mobility.²⁹ IFN- γ also enhanced CD8⁺ T-cell chemotaxis in a paracrine manner as indicated by Huh7 cells stimulated by IFN- γ and TNF- α , causing significantly enhanced mobility (velocity) of the CD8⁺ T cells (Figure 7D, lanes 1 and 2), probably through the increased production of chemokines by the Huh7 cells. Treatment of the Huh7 cells with 2DG, in addition to stimulation by IFN- γ and TNF- α , resulted in enhanced mobility of the CD8⁺ T cells (Figure 7D, lanes 2 and 3), and this enhanced CD8⁺ T-cell mobility was suppressed by the addition of anti-CXCR3 (Figure 7D, lanes 3 and 4). In the presence of CXCL10, 2DG suppressed the mobility (velocity) of CD8⁺ T cells (Figure 7E).

To assess the effects of treatment with 2DG-PLGA-NPs in cancer cells on the competitive uptake of glucose in cancer cells and CD8⁺ T cells ex vivo, we co-cultured Huh7 cells and CD8⁺ T cells with a membrane separating them, and after changing the medium and subsequently adding 2-(N-[nitrobenz-2-oxa1,3-diazol-4-yl]amino)-2-deoxyglucose (2-NBDG), a fluorescent tracer used

for monitoring glucose uptake, we allowed the cells to culture for 16 hours (Figure 6D). Treatment of the Huh7 cells with 2DG-PLGA-NPs resulted in a significant decrease in 2-NBDG uptake by the Huh7 cells and a significant increase in 2-NBDG uptake by the CD8⁺ T cells in the presence of glucose (Figure 6G and H). Then, we investigated the effects of glucose on the chemotaxis of the CD8⁺ T cells obtained after co-culture with 2DG-PLGA-NP-treated Huh7 cells (4 appeared in Figure 6D). Glucose significantly enhanced the mobility of the CD8⁺ T cells toward CXCL10 (Figure 8A, lanes 1 and 3). In addition, the mobility of CD8⁺ T cells obtained after they were co-cultured with 2DG-PLGA-NP-treated Huh7 cells was greater than it was for those co-cultured with PLGA-treated Huh7 cells, even under the same glucose concentration (Figure 8A, lanes 3 and 4), indicating that the CD8⁺ T cells with increased glucose uptake migrate more vigorously. Treatment of the Huh7 cells with the 2DG-PLGA-NPs did not affect the mobility of Tregs in the presence of glucose and macrophage-derived chemokine (C-C motif chemokine 22 [CCL22]/macrophage-derived chemokine),³⁰ which interacts with the C-C chemokine receptor type 4 (CCR4) expressed on Tregs (Figure 8B). These results suggest that the 2DG-PLGA-NPs potentially increased T-cell trafficking in the tumor microenvironment through decreased lactate production in cancer cells and increased IFN- γ production and glucose uptake by the CD8⁺ T cells.

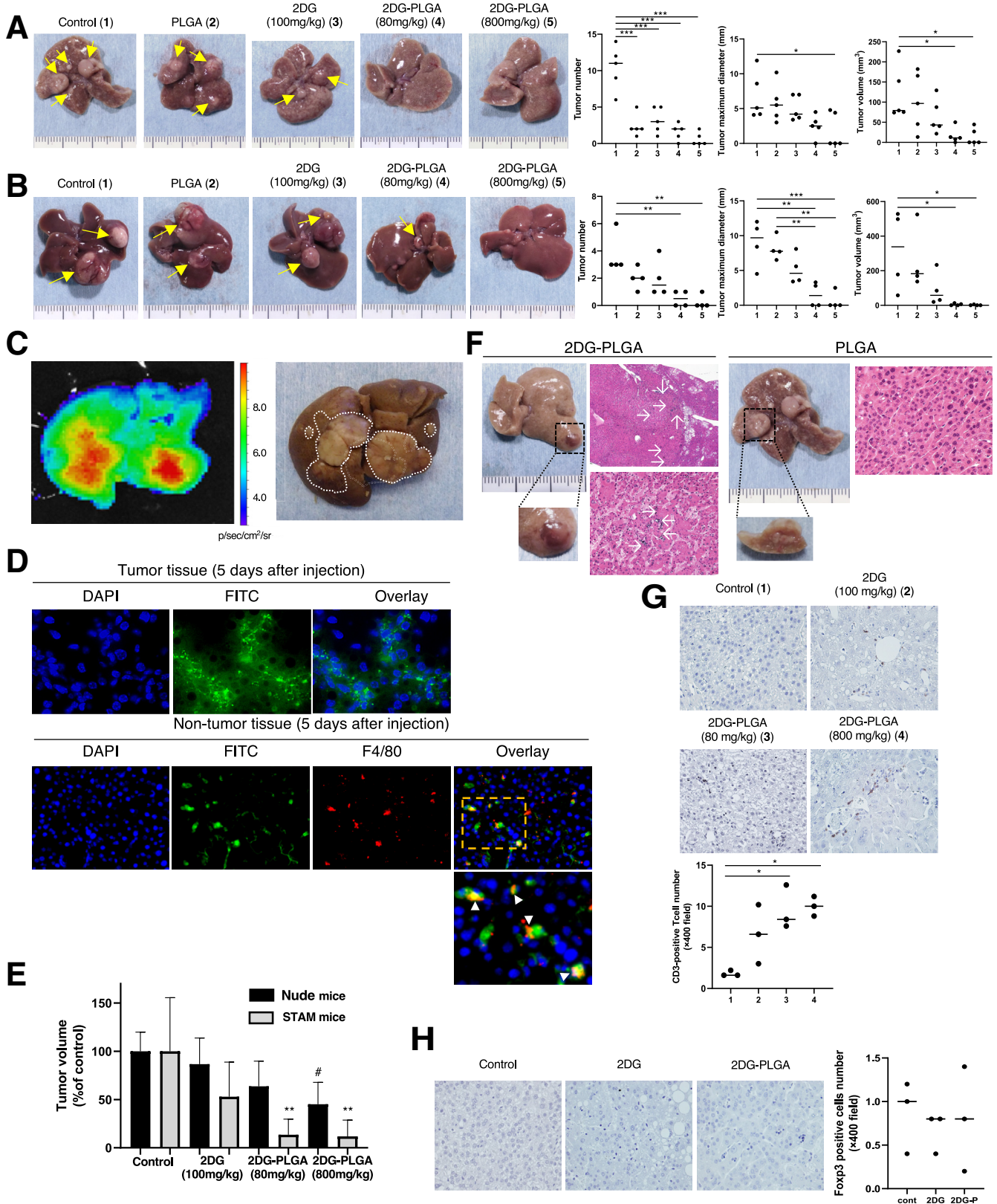
2DG-PLGA-NPs Amplify the Antitumor Effects Induced by Sorafenib and/or Anti-Programmed Death 1 Antibody and Show Antitumor Effects Against Anti-Programmed Death 1-Resistant Tumors

In a phase II trial, pembrolizumab, an anti-programmed death 1 (PD1) monoclonal antibody, showed promising clinical efficacy in patients with advanced HCC who were treated previously with sorafenib, but the effect of a single treatment with pembrolizumab against advanced HCC was not satisfactory.⁹ Based on the effects of the 2DG-PLGA-NPs on CD8⁺ T-cell trafficking into tumors, we hypothesized that 2DG-PLGA-NPs may enhance the expression of PD1-positive T cells in tumors and augment the antitumor effect of an anti-PD1 antibody. As expected, treatment with

Figure 3. (See previous page). Effects of 2DG or 2DG-PLGA-NPs on cell cycle, apoptosis, and ER stress. (A) Cell-cycle distribution of the Huh7 cells (1×10^5) and HepG2 cells (1×10^5) was analyzed for cell cycle using a FACS flow cytometer. * $P < .05$, ** $P < .01$. (B) Huh7 and HepG2 cells were cultured in 96-well plates at a density of 3×10^3 cells/well, and incubated with 2DG (0, 0.2, 1, or 5 mmol/L) for 24 hours. GSH production was measured using a GSSG/GSH quantification kit according to the manufacturer's instructions. * $P < .05$, ** $P < .01$. (C) Terminal deoxynucleotidyl transferase-mediated deoxyuridine triphosphate nick-end labeling (TUNEL) staining for detecting fragmented DNA, and (D) immunostaining for detecting cleaved caspase 3 in the Huh7 cell xenograft tumors 21 days after the commencement of treatment in the 5 groups as indicated ($n = 3$ for each group) (original magnification: $\times 400$). Administration frequency was daily for 2DG (intraperitoneal) and weekly for 2DG-PLGA-NPs (intravenous). Positively stained cells were quantified as described in Figure 2D. * $P < .05$, ** $P < .01$, and *** $P < .001$. Column 1, control; column 2, 2DG (100 mg/kg); column 3, 2DG (1000 mg/kg); column 4, 2DG-PLGA-NP (80 mg/kg); and column 5, 2DG-PLGA-NP (800 mg/kg). (E) Huh7 cell xenograft tumors and growth curves of the mice 21 days after the commencement of the treatment in 3 groups (control, 2DG [1000 mg/kg], and 2DG and 4-PBA [500 mg/kg]) ($n = 5$ for each group). Administration frequency was daily for 2DG (intraperitoneal) and 4-PBA. ** $P < .01$ vs the control and 2DG + 4-PBA. dUTP, 2'-Deoxyuridine, 5'-Triphosphate; 4-PBA; 4-phenylbutyric acid.

2DG-PLGA-NPs resulted in a significant increase in PD1-positive cells in liver tumors of STAM mice than what was obtained with no treatment or 2DG administration, but

the 2DG-PLGA-NP treatment did not affect the expression of programmed death-ligand 1 (PD-L1)-positive cells (Figure 8C). Combined treatment with 2DG-PLGA-NP and



the anti-PD1 antibody resulted in a significant reduction in liver tumor growth in STAM mice (Figure 8D), with significant T-cell infiltration compared with that in the mice with no treatment, treatment with anti-PD1 antibody alone, or treatment with anti-PD1 antibody and 2DG (Figure 8E).

We next investigated the antitumor effects of 2DG-PLGA-NPs in syngeneic mice harboring anti-PD1-resistant tumors. Treatment with 2DG-PLGA-NPs resulted in a significant reduction in tumor growth compared with the level in the mice treated with the isotype control, PLGA alone, or anti-PD1 antibody treatment (Figure 8F). The syngeneic mice were injected intraperitoneally with either an anti-CXCR3 antibody or hamster IgG (isotype control) 5 times during 12 days after the tumors reached 100–150 mm³ in volume (Figure 9A). The administration of anti-CXCR3 with 2DG-PLGA-NPs abrogated the reduction in tumor growth induced by the 2DG-PLGA-NPs and isotype control, but these tumors showed a significant reduction in tumor growth compared with those subjected to the isotype control or anti-CXCR3 (Figure 9B), probably because of the cytotoxic effects of the 2DG-PLGA-NPs. Likewise, T-cell infiltration in tumors, as induced by 2DG-PLGA-NPs, was abrogated by anti-CXCR3 administration (Figure 9C).

The combination therapy of 2DG-PLGA-NPs and sorafenib significantly suppressed the growth of the xenograft tumors in nude mice, compared with the growth in mice treated with nothing (control), PLGA alone, PLGA and sorafenib, or 2DG alone (Figure 9D). Notably, the combination therapy of 2DG-PLGA-NPs and sorafenib did not lead to any adverse effects in terms of body weight, diet consumption, liver weight, or biochemical markers compared with these effects in mice treated with PLGA, 2DG-PLGA-NPs, or a combination of PLGA with sorafenib (Figure 9E). In contrast, the combination therapy of 2DG and sorafenib induced

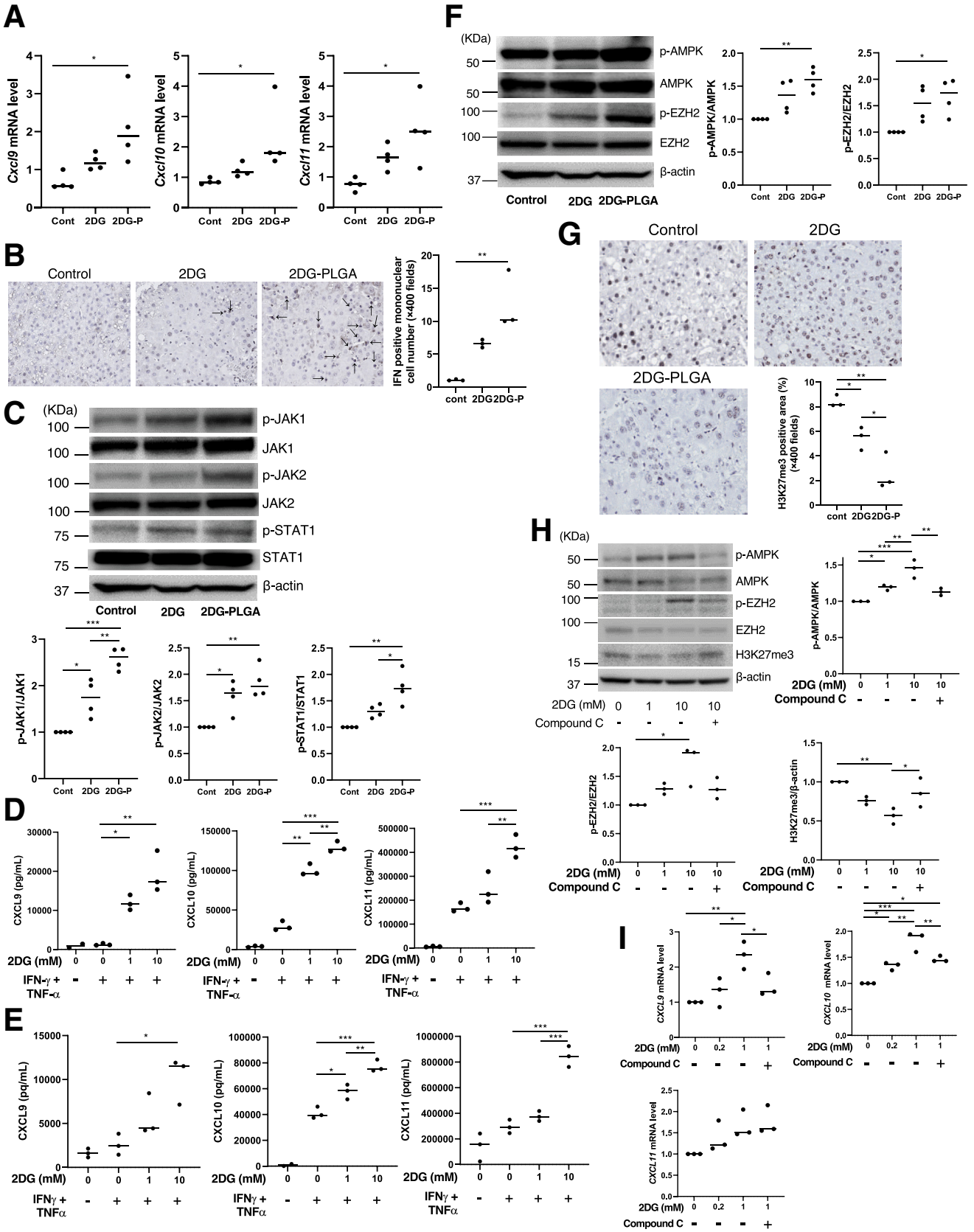
significant body weight loss compared with the effects induced by control, PLGA, 2DG-PLGA-NPs, or a combination of 2DG-PLGA-NPs and sorafenib. These results suggest that the 2DG-PLGA-NPs and sorafenib treatment induced fewer adverse effects than 2DG and sorafenib treatment.

Discussion

We obtained the following results in this study: (1) liver tumor-specific inhibition of glycolysis can be induced by using nanoparticle-mediated delivery of the glucose analog 2DG; (2) the mechanisms by which the inhibition of tumor glycolysis activates T-cell trafficking in the tumor microenvironment were clarified, and (3) the dual effects of cytotoxicity and antitumor immunity were realized against liver tumors by administering 2DG-PLGA-NPs in mice, which has potential for clinical application.

Considering the delivery of 2DG-PLGA-NPs to HCC tissue, it is a practical concern to discern whether the 2DG-PLGA-NPs are not delivered to nontumorous hepatocytes in the presence of cirrhotic sinusoidal endothelial cells. Capillarization of liver sinusoidal endothelial cells, accompanied by the disappearance of the fenestrae and the development of basement membrane, occurs during the progression of chronic liver diseases.³¹ This evidence suggests that 2DG-PLGA-NPs are unlikely to be delivered to the nontumorous cirrhotic hepatocytes. Another practical concern is the extent to which 2DG is effectively taken up by HCC cells. The hepatic accumulation rate of ¹⁸F-2-fluoro-2-deoxyglucose (¹⁸F-FDG), according to ¹⁸F-FDG positron emission tomography results, was reported to be approximately 50% in well-differentiated HCC, and was attributed to the high activity of glucose-6-phosphatase in HCC.³² However, the accumulation of ¹⁸F-FDG was much higher in moderately and poorly differentiated HCC cells and sorafenib-resistant

Figure 4. (See previous page). Effects of 2DG-PLGA-NPs on liver tumor suppression and T-lymphocyte infiltration in immunocompetent mice. (A) Liver tumors in STAM mice treated with nothing (control) (1), PLGA (800 mg/kg) (2), 2DG (100 mg/kg) (3), or 2DG-PLGA-NPs (80 mg/kg [4] or 800 mg/kg [5]) for 3 weeks. Administration frequency was daily for 2DG (intraperitoneal) and weekly for PLGA and 2DG-PLGA-NPs (intravenous). Yellow arrows indicate liver tumors (n = 5 for each group). **P* < .05, ****P* < .001. (B) Liver tumors in the DEN-treated mice at 8 months of age treated with nothing (control) (1), PLGA (800 mg/kg) (2), 2DG (100 mg/kg) (3), or 2DG-PLGA-NPs (80 mg/kg [4] or 800 mg/kg [5]) for 4 weeks. Administration frequency was daily for 2DG (intraperitoneal) and weekly for PLGA and 2DG-PLGA (intravenous). Yellow arrows indicate the liver tumors (n = 4 for each group). **P* < .05, ***P* < .01, and ****P* < .001. (C) Ex vivo distribution of accumulated ICG in the excised liver from an 8-month-old, DEN-treated mouse 7 days after ICG-PLGA-NP injection, as observed using an in vivo imaging system (left panel). Liver tumors in the excised liver from the DEN-treated mouse used for in vivo imaging system analysis (right panel). White dotted lines indicate liver tumors. (D) FITC accumulation in tumor tissue and nontumor tissue of 13-week-old STAM mouse liver 5 days after the FITC-PLGA-NP injection. DAPI and F4/80 stain the nucleus and the Kupffer cells, respectively. Boxed area is enlarged below. White arrowheads indicate yellow puncta, which suggest FITC accumulation in Kupffer cells. (E) Relative tumor volume compared with that of control for 4 groups of nude mice and STAM mice. ***P* < .01 vs control for STAM mice. #*P* < .05 vs control for nude mice. (F) Liver tumor and its histology showing increased cellular density and thickened trabeculae (H&E, original magnification: ×400) in a STAM mouse that had weekly intravenous injections of PLGA (800 mg/kg) for 3 weeks (right panel). Necrotic liver tumor histology showing mononuclear cell infiltration (indicated by white arrows) and degenerative and/or necrotic hepatocytes (H&E, original magnification, ×40 and ×400) in a STAM mouse that had weekly intravenous injections of 2DG-PLGA-NPs (800 mg/kg) for 3 weeks (left panel). (G) Immunostaining for CD3-positive cells in the liver tumors of STAM mice treated for 3 weeks, in 4 groups as indicated (n = 3 for each group) (original magnification: ×400). Administration frequency was daily for 2DG (intraperitoneal) and weekly for 2DG-PLGA-NPs (intravenous). National Institutes of Health image analysis software was used to quantify the mean percentage of the positively stained area of 5 randomly selected fields in the digital images of each tumor. **P* < .05. (H) Immunostaining for Foxp3-positive cells in the liver tumors of STAM mice at 16 weeks of age previously treated with nothing (control), 2DG (100 mg/kg), or 2DG-PLGA-NPs (800 mg/kg) for 3 weeks (n = 3 for each group) (original magnification, ×400). Administration frequency was daily for 2DG (intraperitoneal) and weekly for 2DG-PLGA-NPs (intravenous). Positively stained cells were quantified as described in panel G.



HCC cells.^{32,33} Thus, 2DG-PLGA-NPs are expected to be good therapeutic agent candidates for patients with advanced HCC. In addition, ¹⁸F-FDG-positron emission tomography can be a companion diagnosis for predicting or monitoring treatment efficacy of 2DG-PLGA-NPs because ¹⁸F-FDG is a radioactive tracer of 2DG.

Increases in tumor glycolysis and lactate production have been reported to blunt T-cell-mediated antitumor immunity in the tumor microenvironment of melanoma.^{7,8} In these studies, reduced levels of CXCL10 in highly glycolytic melanoma cells⁷ and lactate-derived down-regulation of IFN- γ production in T and natural killer cells⁸ were shown. The transcription factors involved in IFN- γ transcription were nuclear factor of activated T cells and nuclear factor- κ B proteins.³⁴ Lactate has been shown to down-regulate nuclear factor of activated T cells, which is critical for the suppression of IFN- γ expression in T cells.⁸ In agreement with these reports, we showed that the inhibition of tumor glycolysis by 2DG-PLGA-NPs restored antitumor immunity through increased T-cell trafficking induced by the enhanced IFN- γ production in T cells and augmented chemokine production in tumors. This study shows that inhibition of tumor glycolysis enhanced the production of CXCL9/CXCL10/CXCL11 in CD8⁺ T cells in an IFN- γ -dependent autocrine manner and in tumor cells in an IFN- γ -dependent paracrine manner. In addition, the inhibition of tumor glycolysis increased the production of CXCL9/CXCL10 through the AMPK-EZH2-H3K27me3 pathway independent of IFN- γ . The IFN- γ -independent mechanisms underlying the enhanced production of CXCL11 by 2DG remain to be elucidated. Aerobic glycolysis also is required for optimal effector function in T cells,^{35,36} and tumor-imposed glycolytic restriction mediates T-cell dysfunction during cancer progression.³⁷ We found that CD8⁺ T cells had increased the glucose uptake when co-cultured with 2DG-PLGA-NP-treated Huh7 cells compared with that in cells co-cultured with PLGA-treated Huh7 cells. These results suggest that CD8⁺ T cells potentially restore the

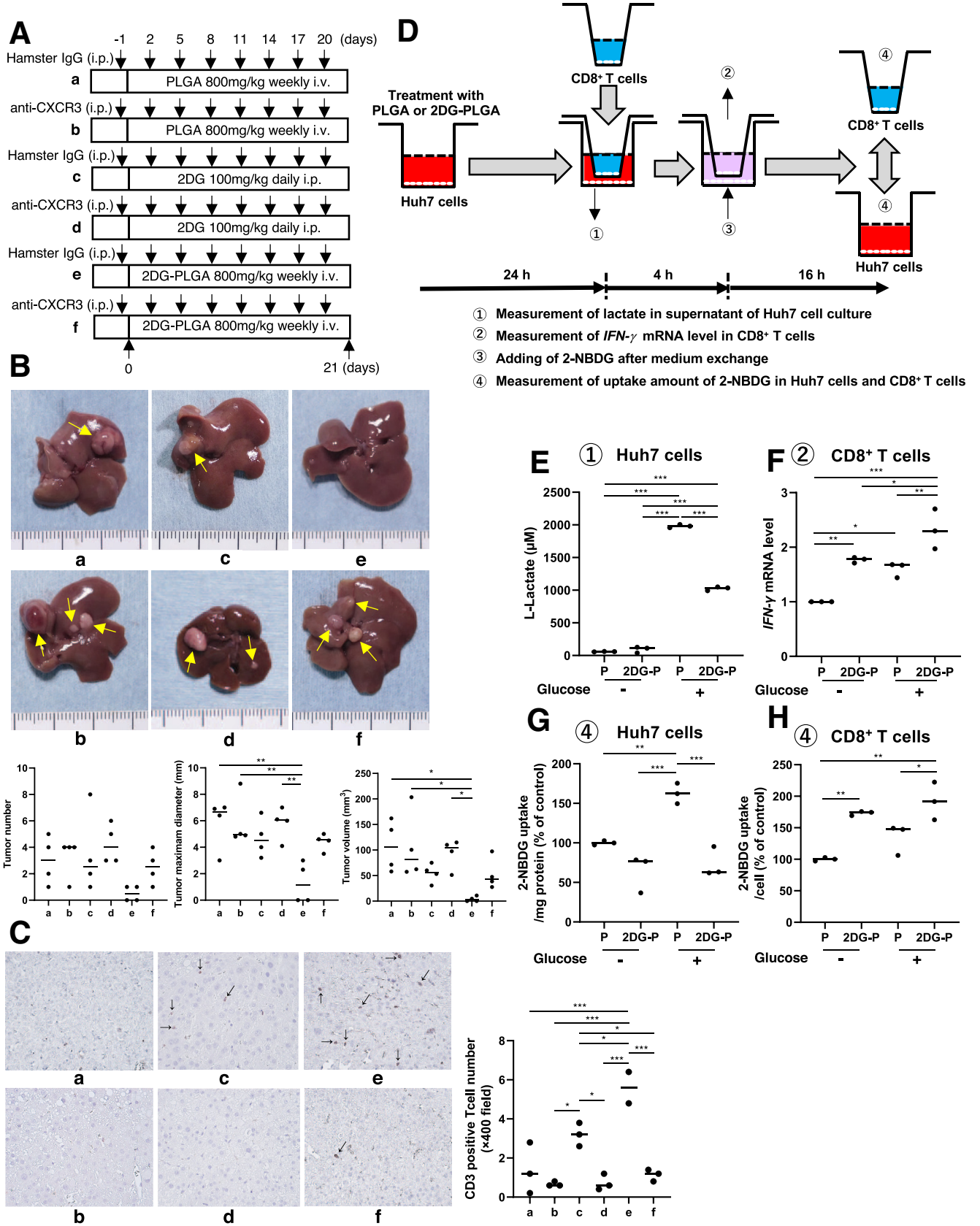
glucose uptake in the tumor microenvironment where tumor cells have suppressed glycolysis.

Combination therapy with 2DG-PLGA-NPs and other therapeutic agents seems to be a reasonable possibility because of the limited therapeutic effect of 2DG itself and the adverse events induced by 2DG in clinical trials.³⁸ The increased aggregation of PD1-positive mononuclear cells and T cells in liver tumors, as induced by the 2DG-PLGA-NPs, accounted for synergistic or additional antitumor effects of a combination therapy with 2DG-PLGA-NPs and anti-PD1 antibodies. The 2DG-PLGA-NPs showed the dual effects of cytotoxicity and antitumor immunity against anti-PD1-resistant tumors because T-cell trafficking abrogation by the anti-CXCR3 neutralizing antibody did not completely, but partially, attenuated the antitumor effects of the 2DG-PLGA-NPs, suggesting a role for cytotoxicity in the antitumor effect induced by 2DG-PLGA-NPs.

Finally, there were at least 2 limitations in this study. First, we could not determine the 2DG concentrations in the tumor tissues. It is necessary to prove that the nanoparticle-mediated delivery of 2DG results in greater concentrations of 2DG in the tumor tissues than is realized by direct delivery of 2DG, regardless of the extremely low loading rate (8%) of 2DG into the 2DG-PLGA-NPs. Second, we could not determine how 2DG was delivered to cancer cells in the tumor microenvironment (2DG transport via glucose transporter or endocytosis of 2DG-PLGA-NPs). Further studies are required to clarify these issues.

In conclusion, 2DG-PLGA-NPs showed cytotoxic effects via oxidative stress, ER stress, and inactivation of mTOR (Figure 10). In addition, 2DG-PLGA-NPs activated CD8⁺ T-cell chemotaxis in the tumor microenvironment via the decreased production of lactate in tumors, the increased IFN- γ production and glucose uptake in CD8⁺ T cells, and production of CXCL9/CXCL10/CXCL11 in both the tumors and CD8⁺ T cells (Figure 10). As a result, 2DG-PLGA-NPs amplified the antitumor effect of anti-PD1 or sorafenib, and

Figure 5. (See previous page). Enhanced chemokine production induced by 2DG-PLGA-NPs and its mechanisms. (A) mRNA levels of *Cxcl9/Cxcl10/Cxcl11* in liver tumors of STAM mice treated with nothing (control), 2DG (100 mg/kg), or 2DG-PLGA-NPs (2DG-P) (800 mg/kg) ($n = 4$ for each group). Administration frequency was daily for 2DG (intraperitoneal) and weekly for 2DG-PLGA-NPs (intravenous). * $P < .05$. (B) Immunostaining for IFN- γ -positive mononuclear cells in the liver tumors of STAM mice treated with nothing (control), 2DG (100 mg/kg), or 2DG-PLGA-NPs (800 mg/kg) ($n = 3$ for each group) (original magnification: $\times 400$). Administration frequency was daily for 2DG (intraperitoneal) and weekly for 2DG-PLGA-NPs (intravenous). Black arrows indicate IFN- γ -positive mononuclear cells. Positively stained cells were quantified as described in Figure 4G. ** $P < .01$. (C) Immunoblots showing p-JAK1, JAK1, p-JAK2, JAK2, p-STAT1, and STAT1 using the liver tumors indicated in panel A. Amounts of phosphorylated protein was normalized to total protein. * $P < .05$, ** $P < .01$, and *** $P < .001$. CXCL9/CXCL10/CXCL11 levels in the culture medium of the (D) Huh7 cells and (E) HepG2 cells. Both cells were incubated with or without 2DG (1 or 10 mmol/L) for 24 hours, with or without the addition of IFN- γ (100 ng/mL) and TNF- α (50 ng/mL) for the final 12 hours of the experiment ($n = 3$ times). * $P < .05$, ** $P < .01$, and *** $P < .001$. (F) Immunoblots showing p-AMPK, AMPK, p-EZH2, and EZH2 for the liver tumors indicated in panel A. Amounts of phosphorylated protein were normalized to total protein. * $P < .05$, ** $P < .01$. (G) Immunostaining for H3K27me3-positive cells in the liver tumors shown in panel B ($n = 3$ for each group) (original magnification: $\times 400$). Positively stained cells were quantified as described in Figure 4G. * $P < .05$, ** $P < .01$. (H) Immunoblots showing p-AMPK, AMPK, p-EZH2, and EZH2 from the Huh7 cells (5×10^5) that were incubated with or without compound C (5 mmol/L) for 48 hours in the absence or presence of 2DG (1 or 10 mmol/L). The amount of H3K27me3 was normalized to that of β -actin. Amounts of phosphorylated protein were normalized to total protein. * $P < .05$, ** $P < .01$, and *** $P < .001$. (I) mRNA levels of *CXCL9/CXCL10/CXCL11* in the Huh7 cells incubated with or without 2DG for 48 hours in the absence or presence of compound C ($n = 3$ times). * $P < .05$, ** $P < .01$, and *** $P < .001$. Cont, control.



showed an antitumor effect against anti-PD1-resistant tumors.

Materials and Methods

PLGA Nanoparticles

Preparation of PLGA nanoparticles. PLGA, with an average molecular weight of 20,000 and a copolymer ratio of lactic acid to glycolide of 75:25 (Wako Pure Chemical Industries, Ltd, Osaka, Japan), was used as a matrix for the nanoparticles, and polyvinyl alcohol (The Nippon Synthetic Chemical Industry, Co, Ltd, Osaka, Japan) was used as a dispersing agent. PLGA nanoparticles incorporated with 2DG (Wako Pure Chemical Industries, Ltd) (2DG-PLGA-NP), ICG (Dojin Chemical, Tokyo, Japan) (ICG-PLGA-NP), or FITC (Dojin Chemical) (FITC-PLGA-NP) were prepared using an ULREA SS-11 (Technique, Co, Ltd, Osaka, Japan). First, liquid A was filled in a liquid A tank, and the tank was pressurized to 0.3 MPa. Subsequently, liquid A was transferred at a set value of 43°C and at a rate of 167 mL/min, and, thereafter, liquid B was transferred at a set value of 41°C and at a rate of 100 mL/min. Liquid A is an aqueous solution containing 0.5% polyvinyl alcohol. Liquid B for 2DG-PLGA-NP is a solution containing PLGA, 2DG, acetone, and ethanol in a weight ratio of 0.65:0.25:66.1:33. In contrast, liquid B for ICG-PLGA-NP is a solution containing PLGA, ICG, acetone, and ethanol in a weight ratio of 0.65:0.1:66.2:33.1. The number of revolutions was adjusted to 1000 rpm and the back pressure was adjusted to 0.02 MPa. After collecting the discharge liquid for the proper period, the solvents contained in the discharge liquid were removed by distillation using an evaporator. The resulting aqueous 2DG-PLGA-NP and ICG-PLGA-NP dispersion were freeze-dried. In the case of FITC-PLGA-NP, liquid A is an aqueous solution containing 2.0% polyvinyl alcohol and liquid B is a solution containing PLGA, FITC, acetone, and ethanol in a weight ratio of 4.0:0.2:63.8:31.9. Liquid A was transferred at a rate of 120 mL/min, and, thereafter, liquid B was transferred at a rate of 100 mL/min. The other conditions for preparing FITC-PLGA-NP by ULREA SS-11 was the same as described earlier. After collecting the discharge liquid for the proper period, post-treatment of the discharge liquid was performed as previously described.³⁹

Characterization of PLGA nanoparticles. The volume-based particle size and zeta potential of PLGA-NPs, 2DG-PLGA-NPs, ICG-PLGA-NPs, and FITC-PLGA-NPs were

measured using a laser light diffraction and scattering method (Nanotracer Wave EX150 and Nanotracer Wave UZ152, respectively, MicrotracBEL, Co, Osaka, Japan). The morphology of the nanoparticles was observed using a transmission electron microscope (JEM-1400; JEOL, Ltd, Tokyo, Japan). Ten milligrams of nanoparticles were dispersed in 10 mL distilled water and samples were suspended by vortex mixer for 30 seconds. The suspension of nanoparticles (1 mg/mL) was deposited onto copper grids covered with formvar film (100 mesh). Negative staining with uranyl acetate 2% (w/v) was performed to observe PLGA-NPs, 2DG-PLGA-NPs, ICG-PLGA-NPs, and FITC-PLGA-NPs.

Nanoparticles (20 mg) were dispersed in 10 mL distilled water. The mixture solution was stirred and subjected to an ultrasonic treatment for 30 minutes. After 1 mL acetonitrile was added to 1 mL of the mixture solution, samples were centrifuged at $10,000 \times g$ for 15 minutes, and the filtered supernatant was subjected to measurement of the content of 2DG, ICG, and FITC. The content of 2DG, ICG, and FITC was quantified using an evaporative light-scattering detector system (Shimadzu, Co, Kyoto, Japan), an Ultraspec2100 Pro spectrophotometer (GE Healthcare, Buckinghamshire, UK), and a fluorophotometer (Infinite M200 PRO; Tecan, Grödig, Austria), respectively. The loading capacity was calculated by dividing the content of each encapsulated substance (2DG, ICG, or FITC) by the total nanoparticle weight.

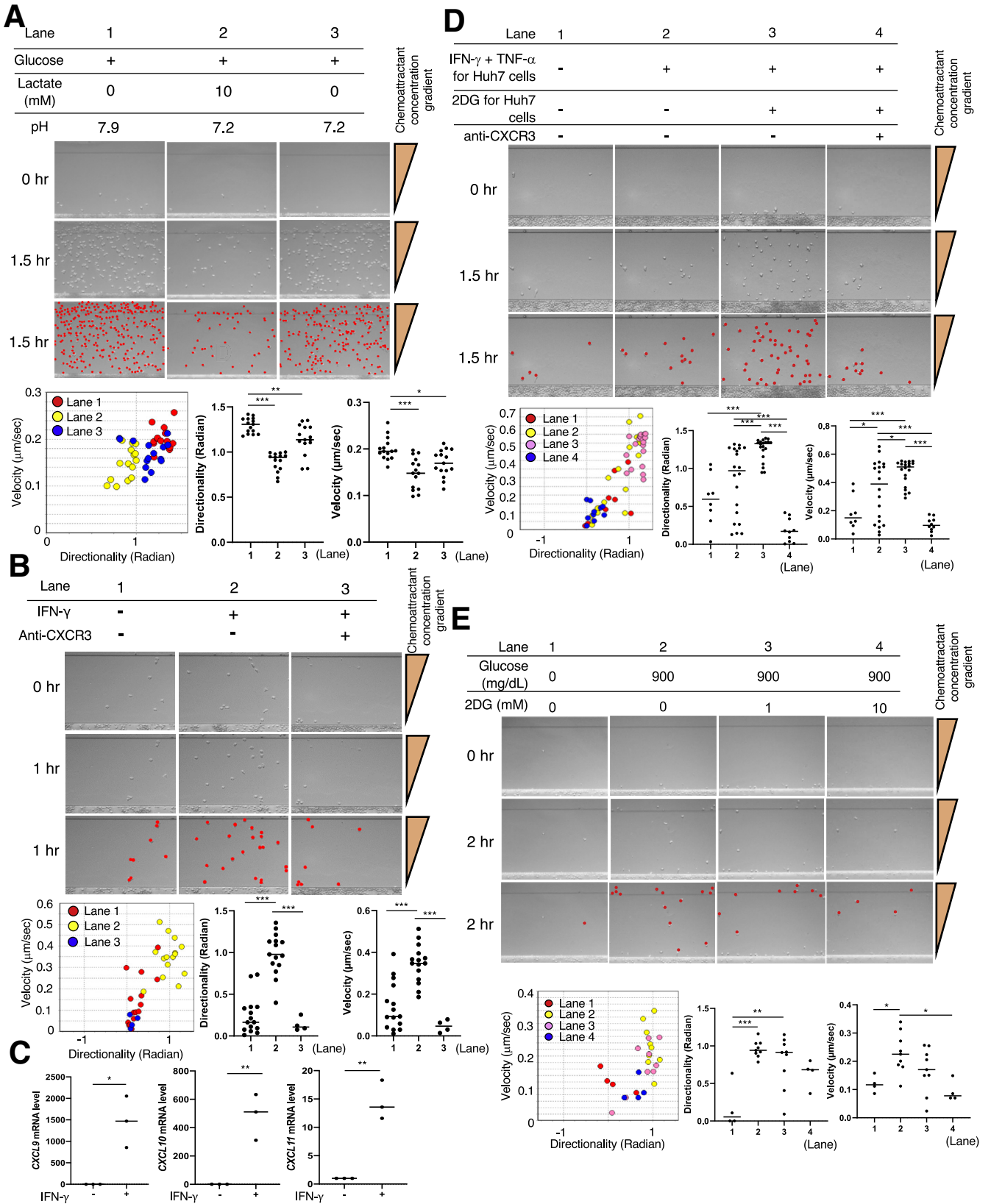
Animals and Experimental Design

We used nude mice with xenograft tumors, C57BL6/J-based HCC mouse models (a nonalcoholic steatohepatitis-related HCC mouse model [STAM mouse; SMC Laboratories, Inc, Tokyo, Japan], and a DEN-induced HCC mouse model), and a syngeneic mouse model transplanted with B16F10 cells⁴⁰ (1×10^7 , anti-PD1 antibody-resistant melanoma cells).

Assessment of 2DG-PLGA-NPs for In Vivo Delivery.

Six-week-old male nude mice (BALB/c-nu/nu) received subcutaneous injections of 1×10^7 Huh7, HepG2, HT29, OS-RC-2, or BxPC3 cells. When the xenograft tumors reached a maximum diameter of 15 mm, 3 mice were injected with ICG-PLGA-NPs (800 mg/kg) or FITC-PLGA-NPs (800 mg/kg) through the cervical vein. The in vivo distribution of ICG accumulation was assessed in the mice under inhalation anesthesia with isoflurane 1.5, 6, and 24 hours, and 2, 3, 7,

Figure 6. (See previous page). Neutralization of chemokine receptor CXCR3 and co-culture experiments with CD8⁺ T cells and Huh7 cells. (A) Schematic of the treatment used in the DEN-induced HCC mouse models. (B) Liver tumors in the DEN-induced HCC mouse models treated as shown in panel A ($n = 4$ for each group). Yellow arrows indicate liver tumors. $*P < .05$, $**P < .01$. (C) Immunostaining for CD3-positive cells in the liver tumors of the DEN-induced HCC mouse models in groups, as shown in panel A ($n = 3$ for each group) (original magnification: $\times 400$). Black arrows indicate CD3-positive T cells. Positively stained cells were quantified as described in Figure 4G. $*P < .05$, $***P < .001$. (D) Schematic of the experiments of human CD8⁺ T cells co-cultured with Huh7 cells treated with 2DG-PLGA-NPs or PLGA. (E) Lactate levels in the supernatant of the Huh7 cell culture treated with 2DG-PLGA-NPs (equivalent to 10 mmol/L 2DG) or PLGA (same weight as 2DG-PLGA) for 24 hours in the absence or presence of glucose (900 mg/dL). $***P < .001$. (F) *IFN- γ* mRNA levels in the CD8⁺ T cells co-cultured with the Huh7 cells treated with 2DG-PLGA-NPs or PLGA for 4 hours in the absence or presence of glucose (900 mg/dL). $*P < .05$, $**P < .01$, and $***P < .001$. 2-NBDG uptake in the (G) Huh7 cells and (H) CD8⁺ T cells after CD8⁺ T cells were co-cultured with Huh7 cells treated with 2DG-PLGA-NPs or PLGA for 16 hours in the absence or presence of glucose (900 mg/dL). $*P < .05$, $**P < .01$, and $***P < .001$. i.p., intraperitoneal injection; i.v., intravenous injection.



and 10 days after injection of ICG-PLGA-NPs, using an in vivo imaging system (PerkinElmer, Inc, Waltham, MA). FITC accumulation in the tumor tissue was assessed by fluorescence microscopy (BZ-9000; KEYENCE, Osaka, Japan) after the mice were killed, 3 and 7 days after FITC-PLGA-NP injection.

Nine-month-old male DEN-treated mice were injected with ICG-PLGA-NPs (80 mg/kg), killed 7 days after injection of ICG-PLGA-NPs, and the distribution of ICG accumulation in the excised liver was assessed, using an in vivo imaging system. Similarly, 16-week-old male STAM mice were injected with FITC-PLGA-NPs (800 mg/kg), and FITC accumulation in tumor tissue and nontumor tissue of the excised liver was assessed by fluorescence microscopy 5 days after FITC-PLGA-NP injection.

Nude mice with xenograft tumors. When the xenograft tumors reached a size of 100–150 mm³, the mice were administered 2DG (100 mg/kg or 1000 mg/kg, by intraperitoneal injection) daily, 2DG-PLGA-NPs (80 mg/kg or 800 mg/kg, by intravenous injection), or PLGA (800 mg/kg, by intravenous injection) weekly for 3 weeks. Some mice were administered 2DG (1000 mg/kg) daily with 4-phenylbutyric acid (500 mg/kg) (Sigma-Aldrich, St. Louis, MO) or were administered 2DG-PLGA-NPs (800 mg/kg) or PLGA (800 mg/kg) weekly with or without daily administration of sorafenib (5 mg/kg) by gastric intubation for 3 weeks. Tumor size (*V*) was calculated using the following formula: $V \text{ (mm}^3\text{)} = \text{width (mm)}^2 \times \text{length (mm)}/2$. Body weight and tumor size were measured every 3 days, and dietary intake was measured every 7 days.

Immunocompetent HCC mouse models. STAM mice were generated as described previously.⁴¹ Thirteen-week-old male STAM mice were intraperitoneally administered 2DG (100 mg/kg) daily or intravenously administered 2DG-PLGA-NPs (80 mg/kg or 800 mg/kg) or PLGA (800 mg/kg) weekly for 3 weeks. Some of the 13-week-old STAM male mice were administered 2DG (100 mg/kg) daily every 3 days via intraperitoneal injection of an anti-PD1 antibody (200 μg) (Bio X Cell, West Lebanon, NH), weekly administered 2DG-PLGA-NPs (800 mg/kg) every 3 days via

intraperitoneal injection of an anti-PD1 antibody, or intraperitoneally injected with anti-PD1 antibody or rat IgG2a (Bio X Cell) (isotype control) every 3 days for 3 weeks. Fifteen-day-old male C57BL6/J mice were injected with DEN (100 μg/mouse) (Sigma-Aldrich), and 8 months after the first DEN injection, they were intraperitoneally administered 2DG (100 mg/kg) daily or intravenously administered 2DG-PLGA-NPs (80 mg/kg or 800 mg/kg) or PLGA (800 mg/kg) weekly for 4 weeks. As syngeneic mouse models, the C57BL6/J mice that had been injected with B16F10 cells (anti-PD1-resistant melanoma cells), and when the tumors reached a size of 100–150 mm³ the mice were given a daily intraperitoneal injection of 2DG (100 mg/kg), a weekly intravenous injection of 2DG-PLGA-NPs (800 mg/kg) or PLGA (800 mg/kg), or an intraperitoneal injection of anti-PD1 antibody or rat IgG2a every 3 days for 12 days.

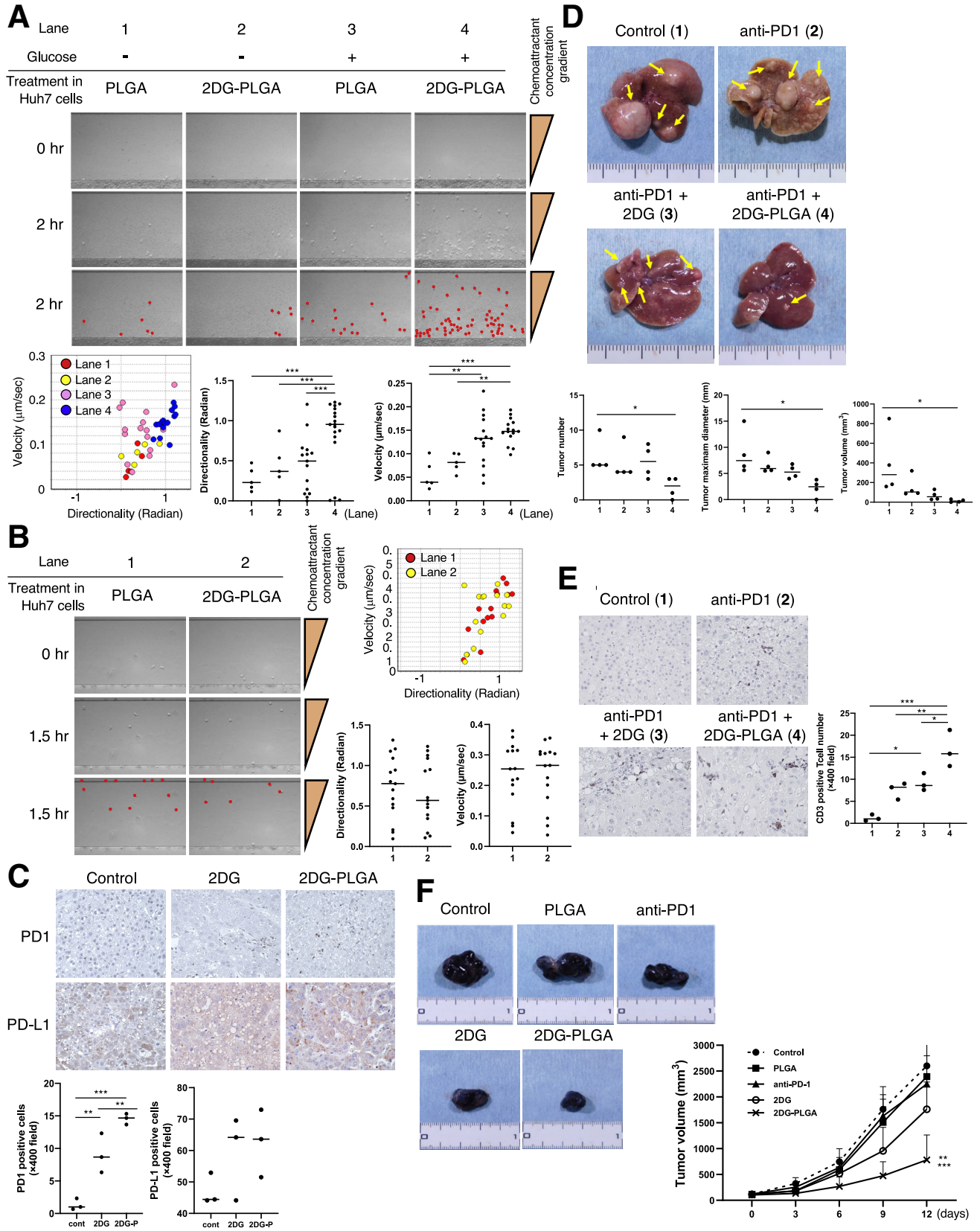
Neutralization of chemokine receptor CXCR3. Eight months after the initial DEN injection, some DEN-treated mice were administered 2DG (1000 mg/kg) daily, 2DG-PLGA-NPs (800 mg/kg) or PLGA (800 mg/kg) weekly for 3 weeks with 8 times intraperitoneal injections of an anti-CXCR3 antibody (200 μg) (Bio X Cell) or hamster IgG (Bio X Cell) (isotype control) (Figure 6A). When tumors reached a size of 100–150 mm³, some syngeneic mice were weekly administered 2DG (1000 mg/kg) daily, 2DG-PLGA-NPs (1000 mg/kg), or PLGA (800 mg/kg) weekly with 5 intraperitoneal injections of anti-CXCR3 antibody (200 μg) or hamster IgG for 12 days (Figure 9A).

The mice were bred and maintained according to the guidelines approved by the Institutional Animal Care Use Committee (Kawasaki Medical School), and killed by carbon dioxide asphyxiation, as approved by the Panel on Euthanasia of the American Veterinary Association. After the mice were killed, tumor tissue and blood samples were collected.

Cell Culture

Huh7 and HepG2 hepatoma cells and B16F10 cells were obtained from the Cell Resource Center for Biomedical

Figure 7. (See previous page). CD8⁺ T-cell and Treg migration in 260-μm-long microchannels. (A) After aligning the CD8⁺ T cells (5×10^4 cells/well) on the edge of a microchannel (*bottom of each panel*), medium containing CXCL10 and glucose (*lane 1*); CXCL10, glucose, and lactate (*lane 2*); or CXCL10, glucose, and hydrochloric acid (*lane 3*) were injected into the compartment opposite site the CD8⁺ T-cell-containing compartment. CD8⁺ T cells in the images (*middle line of each panel*) are represented by *red dots* in each panel in the third line. Migration of the CD8⁺ T cells randomly selected from those in each lane was analyzed using TAXIScan Analyzer 2 software. To obtain statistical data of cell migration, median values of velocity and directionality (direction toward ligands) for each cell within an experimental period were calculated from the migratory pathway data obtained from time-lapse images. Data are expressed in velocity-directionality plots. **P* < .05, ***P* < .01, and ****P* < .001. (B) Migration of the CD8⁺ T cells co-cultured with IFN-γ (1 μg/mL) for 20 hours was analyzed in the same manner as described in panel A except for the injected medium (*lane 1*, none; *lane 2*, culture supernatant of the CD8⁺ T cells with IFN-γ; *lane 3*, culture supernatant of the CD8⁺ T cells with IFN-γ + anti-CXCR3). ****P* < .001. (C) mRNA levels of CXCL9/CXCL10/CXCL11 in the CD8⁺ T cells co-cultured with or without IFN-γ. **P* < .05, ***P* < .01. (D) Huh7 cells (1×10^4 cells/well) that were incubated with or without 2DG (10 mmol/L) for 24 hours, with or without the addition of IFN-γ and TNF-α for the final 12 hours of the experiment, were added into the chemoattractant injection side of the microchannel. CD8⁺ T-cell migration was analyzed in the same manner as described for panel A, except the injected medium was added to the compartment opposite the CD8⁺ T-cell-containing compartment (*lane 1*, none; *lane 2*, none; *lane 3*, none; and *lane 4*, anti-CXCR3). CD8⁺ T cells in the images were generated in the same manner as described in panel A. **P* < .05, ****P* < .001. (E) After aligning the CD8⁺ T cells (5×10^4 cells/well) on the edge of the microchannel (*bottom in each panel*), medium containing CXCL10 (*lane 1*); CXCL10 and glucose (*lane 2*); CXCL10, glucose, and 1 mmol/L 2DG (*lane 3*); or CXCL10, glucose, and 10 mmol/L 2DG (*lane 4*) was injected into the compartment on the opposite side of the CD8⁺ T-cell-containing compartment. The CD8⁺ T cells in the images were drawn in the same manner as described in panel A. **P* < .05, ***P* < .01, and ****P* < .001.



Research of the Institute of Development, Aging and Cancer at Tohoku University (Sendai). HT29 colon cancer cells were purchased from DS Pharma Biomedical, Co, Ltd (Osaka, Japan). BxPC3 (ATCC CRL-CRL-1687) pancreatic cancer cells were purchased from the American Type Culture Collection. OS-RC-2 renal cancer cells were purchased from Bioresources of RIKEN (Saitama). The Huh7, HepG2, B16F10, BxPC3, OS-RC-2, and HT29 cells were cultured in Dulbecco's modified Eagle medium containing 10% fetal bovine serum (FBS), RPMI1640 medium containing 10% FBS, and McCoy's 5A medium containing 10% FBS at 37°C in a humidified atmosphere with 5% CO₂.

Measurement of the ATP Production Rate

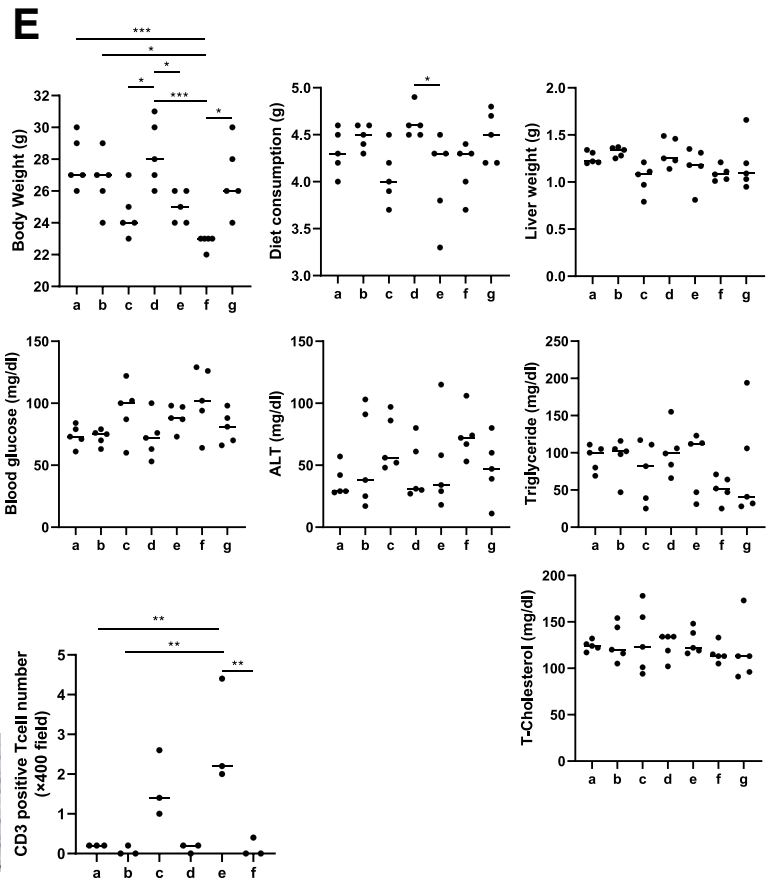
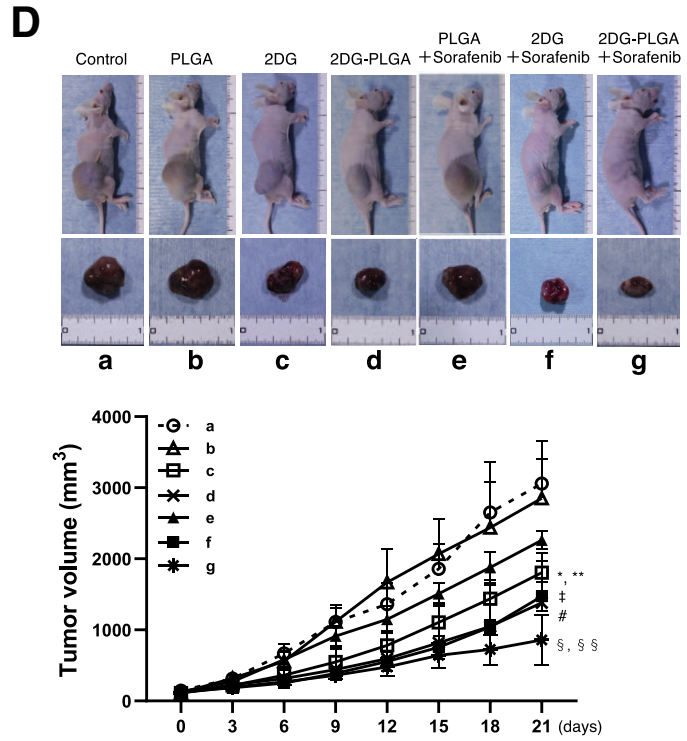
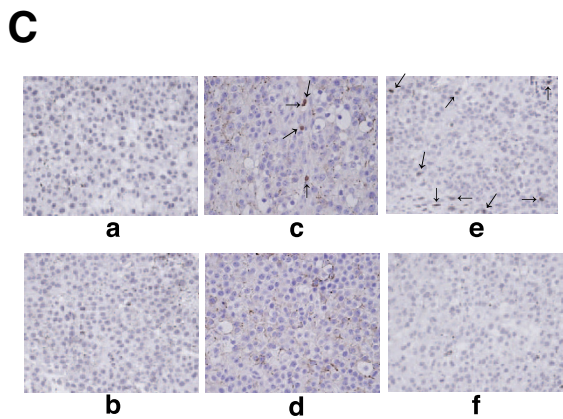
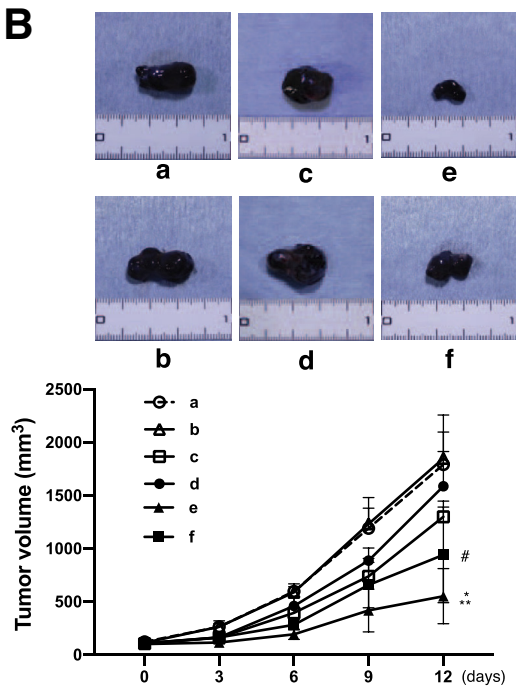
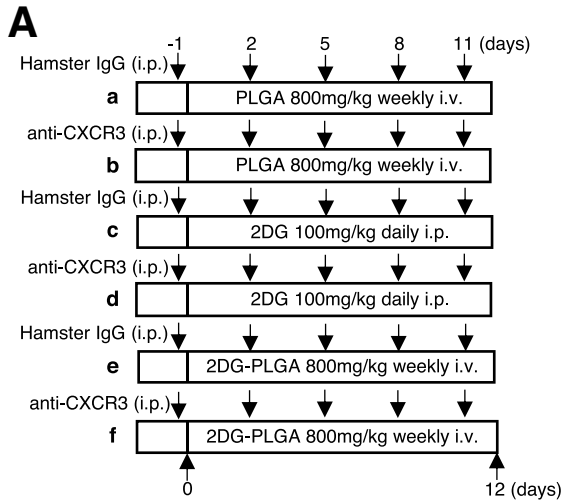
Total, glycolytic, and mitochondrial ATP production rates were measured using an Agilent Seahorse XFp Real-Time ATP Rate Assay kit (Agilent Technologies, Inc, Santa Clara, CA) and a Seahorse XF24 Extracellular Flux Analyzer (Seahorse Bioscience, North Billerica, MA), according to the manufacturer's instructions. The Huh7 cells were cultured in 24-well seahorse plates at a density of 3×10^4 cells/well. The cell culture medium was replaced with Dulbecco's modified Eagle medium containing 10 mmol/L glucose, 1 mmol/L pyruvate, and 2 mmol/L glutamine at pH 7.4. The extracellular acidification rates and oxygen consumption rates were analyzed after an injection of 2DG (0, 1, 5, 10, or 50 mmol/L), 1 μ mol/L oligomycin, 1 μ mol/L carbonyl cyanide 4-(trifluoromethoxy)phenylhydrazone, and 0.5 μ mol/L rotenone/antimycin A. The glycolytic and mitochondrial ATP production rates were determined based on the extracellular acidification rates and oxygen consumption rates using an Agilent Seahorse XFp Real-Time ATP rate assay report generator. The total ATP production rate was determined by adding the glycolytic ATP production rate to the mitochondrial ATP production rate.

Immunoblotting

The cells were harvested using trypsin/ethylenediaminetetraacetic acid, washed in phosphate-buffered saline, and resuspended in cell lysis buffer (Cell Signaling

Technology, Danvers, MA) containing a 1% protease inhibitor mixture (Sigma-Aldrich) and 100 mmol/L phenylmethylsulfonyl fluoride. Tissue samples also were lysed in the same lysis buffer. The proteins in the lysates of cultured cells or tumor tissues were separated by sodium dodecyl sulfate-polyacrylamide gel electrophoresis. These proteins were transferred to polyvinylidene difluoride membranes (Pall Corporation, New York, NY), and blocked for 1 hour at room temperature with 5% bovine serum albumin and 0.1% Tween-20 in Tris-buffered saline. The samples subsequently were incubated overnight at 4°C with the following antibodies: a rabbit anti-phospho-AMPK α (Thr172) monoclonal antibody (Cell Signaling Technology), a rabbit anti-AMPK α monoclonal antibody (Cell Signaling Technology), a rabbit anti-phospho-mTOR (Ser2448) monoclonal antibody (Cell Signaling Technology), a rabbit anti-mTOR monoclonal antibody (Cell Signaling Technology), a rabbit anti-phospho-S6 ribosomal protein (Ser235/236) monoclonal antibody (Cell Signaling Technology), a mouse anti-S6 ribosomal protein monoclonal antibody (Cell Signaling Technology), a rabbit anti-phospho-Rb (Ser780) polyclonal antibody (Cell Signaling Technology), a mouse anti-Rb monoclonal antibody (Cell Signaling Technology), a rabbit anti-spliced x-box binding protein 1 monoclonal antibody (Cell Signaling Technology), a mouse anti-CCAAT/enhancer binding protein-homologous protein monoclonal antibody (Cell Signaling Technology), a rabbit anti-activating transcription factor 4 monoclonal antibody (Cell Signaling Technology), a rabbit anti-cyclin D1 monoclonal antibody (Cell Signaling Technology), a mouse anti-proliferating cell nuclear antigen monoclonal antibody (Santa Cruz Biotechnology, Santa Cruz, CA), a rabbit anti-vascular endothelial growth factor polyclonal antibody (Abcam, Cambridge, UK), a rabbit anti-phospho-JAK1 monoclonal antibody (Cell Signaling Technology), a rabbit anti-JAK1 monoclonal antibody (Cell Signaling Technology), a rabbit anti-phospho-JAK2 monoclonal antibody (Cell Signaling Technology), a rabbit anti-JAK2 monoclonal antibody (Cell Signaling Technology), a rabbit anti-phospho-STAT1 (Tyr701) monoclonal antibody (Cell Signaling Technology), a rabbit anti-STAT1 monoclonal antibody (Cell Signaling Technology),

Figure 8. (See previous page). CD8⁺ T-cell and Treg migration in 260- μ m-long microchannels, and amplification of the antitumor effects of anti-PD1 antibody and suppression of the anti-PD1-resistant tumors by 2DG-PLGA-NPs. (A) Migration of the CD8⁺ T cells co-cultured with 2DG-PLGA-NP- or PLGA-treated Huh7 cells was analyzed in the same manner as described in Figure 7A, except for the injected medium (lane 1, CXCL10; lane 2, CXCL10; lane 3, CXCL10 and glucose; lane 4, CXCL10 and glucose). ***P* < .01, ****P* < .001. (B) CD4⁺/CD25⁺ Tregs (1×10^4 cells/well) co-cultured with 2DG-PLGA-NP- or PLGA-treated Huh7 cells was analyzed in the same manner as described in Figure 7A, except for the injected medium (lanes 1 and 2, CCL22). (C) Immunostaining for PD1 or PD-L1 in the liver tumors of STAM mice treated with nothing (control), 2DG (100 mg/kg), or 2DG-PLGA-NPs (800 mg/kg) (*n* = 3 for each group) (original magnification: $\times 400$). Administration frequency was daily for 2DG (intraperitoneal) and weekly for 2DG-PLGA-NPs (intravenous). Positively stained cells were quantified as described in Figure 4G. ***P* < .01, ****P* < .001. (D) Liver tumors in STAM mice treated with nothing (control) (1), anti-PD1 (2), 2DG (100 mg/kg) + anti-PD1 (3), or 2DG-PLGA-NPs (800 mg/kg) + anti-PD1 (4) for 3 weeks. Administration frequency was every 3 days for anti-PD1, daily for 2DG (intraperitoneal), and weekly for 2DG-PLGA-NPs (intravenous). Yellow arrows indicate liver tumors. **P* < .05. (E) Immunostaining for CD3-positive cells in liver tumors of STAM mice in each group as shown in panel D (*n* = 3 for each group) (original magnification: $\times 400$). Positively stained cells were quantified as described in Figure 4G. **P* < .05, ***P* < .01 and ****P* < .001. (F) Tumors and growth curves of the syngeneic mice transplanted with B16F10 cells (anti-PD1-resistant melanoma cells) treated with rat IgG2a (control), PLGA (800 mg/kg), anti-PD1, 2DG (100 mg/kg) or 2DG-PLGA-NPs (800 mg/kg) for 12 days. Administration frequency was every 3 days for IgG2a and anti-PD1, daily for 2DG (intraperitoneal), and weekly for PLGA and 2DG-PLGA-NPs (intravenous). ***P* < .01 vs PLGA and anti-PD1, ****P* < .001 vs the control. cont, control.



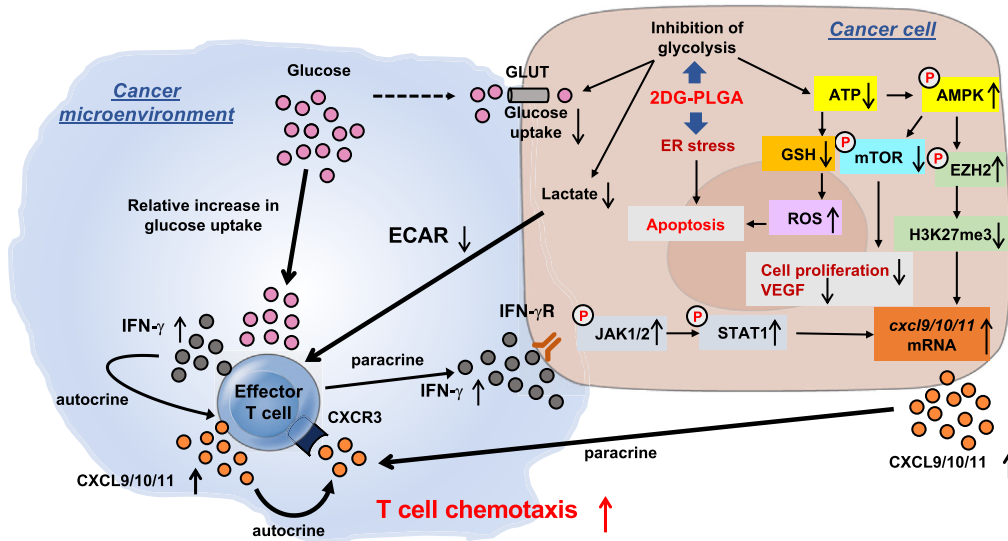


Figure 10. Schematic diagram depicting the mechanisms by which 2DG-PLGA-NPs exert dual antitumor effects of cytotoxicity and antitumor immunity. ECAR, extracellular acidification rate; GLUT, glucose transporter; VEGF, vascular endothelial growth factor.

a rabbit anti-phospho-EZH2 (Thr311) polyclonal antibody (Cell Signaling Technology), a rabbit anti-EZH2 monoclonal antibody (Cell Signaling Technology), and a rabbit anti-trimethyl-histone H3 (Lys27) polyclonal antibody (Sigma-Aldrich). The transferred proteins also were blocked for 1 hour at room temperature with 5% milk and 0.1% Tween-20 in Tris-buffered saline and subsequently were incubated for 1 hour at room temperature with a rabbit anti- β -actin monoclonal antibody (Cell Signaling Technology). Immunoreactive proteins were detected using an enhanced chemiluminescence reagent (Western Lightning Plus-ECL; Perkin-Elmer). Immunoblots for p-AMPK α , AMPK α , p-EZH2, EZH2, and trimethyl-histone H3 were obtained for the Huh7 cells in the presence or absence of the AMPK inhibitor, compound C.

Histologic Procedures

Tumor tissues from mice were fixed in 4% paraformaldehyde in phosphate-buffered saline and embedded in paraffin for histologic analysis. In addition to undergoing H&E staining, the liver sections were incubated overnight with a 1:200 dilution of a rabbit anti-CD34 monoclonal antibody (Abcam), a rabbit anti-cleaved-caspase 3

polyclonal antibody (Biobyte, Ltd, Cambridge, UK), a rabbit anti-CD3 monoclonal antibody (GeneTex, Irvine, CA), a rabbit anti-IFN- γ polyclonal antibody (Abcam), a rat anti-Foxp3 monoclonal antibody (Thermo Fischer Scientific, Waltham, MA), a rabbit anti-trimethyl-histone H3 (Lys27) polyclonal antibody (Merck KGaA, Darmstadt, Germany), a rabbit anti-PD1 polyclonal antibody (Proteintech, Rosemont, IL), and a rabbit anti-PD-L1 polyclonal antibody (Proteintech) at 4°C overnight. After incubation with avidin-conjugated peroxidase (VECTASTAIN Elite ABC; Vector Laboratories, Burlingame, CA), the tissue sections were developed in 3,3'-diaminobenzidine tetrahydrochloride (Sigma Chemical, Co, St. Louis, MO). National Institutes of Health image analysis software was used to quantify the mean percentage area or the mean number of positively stained CD34, cleaved caspase 3, CD3, IFN- γ , FOXP3, trimethyl-histone H3, PD1, or PD-L1 cells in 5 randomly selected fields of view in the digital images of each xenograft tumor or liver tumor. Frozen sections of the xenograft tumors obtained from the FITC-PLGA-NP-injected mice were fixed with Antifade Mounting Medium with 4',6-diamidino-2-phenylindole (DAPI) (Vector Laboratories) and assessed by fluorescence microscopy. In addition,

Figure 9. (See previous page). Neutralization of chemokine receptor CXCR3 and amplification of the antitumor effects of sorafenib by 2DG-PLGA-NPs. (A) Schematic of the treatment of syngeneic mice transplanted with B16F10 cells. (B) Tumors and growth curves of the syngeneic mice treated as shown in panel A ($n = 5$ for each group). * $P < .05$ vs c; ** $P < .01$ vs a, b, and d; # $P < .05$ vs a and b. (C) Immunostaining for CD3-positive T cells in the tumors of the syngeneic mice treated as shown in panel A ($n = 3$ for each group) (original magnification: $\times 400$). Black arrows indicate CD3-positive T cells. Positively stained cells were quantified as described in Figure 4G. ** $P < .01$. (D) Huh7 cell xenograft tumors and growth curves of the mice 21 days after treatment was initiated in 7 groups. Mice without treatment (control) (a), mice with intravenous administration of PLGA (800 mg/kg) weekly for 3 weeks (b), mice with intraperitoneal administration of 2DG (1000 mg/kg) daily for 3 weeks (c), mice with intravenous administration of 2DG-PLGA-NPs (800 mg/kg) weekly for 3 weeks (d), mice with intravenous administration of PLGA (800 mg/kg) weekly and administration of sorafenib [5 mg/kg] daily by gastric intubation for 3 weeks (e), mice with intraperitoneal administration of 2DG (1000 mg/kg) daily and administration of sorafenib (5 mg/kg) daily by gastric intubation for 3 weeks (f), and mice with intravenous administration of 2DG-PLGA-NPs (800 mg/kg) weekly and administration of sorafenib (5 mg/kg) daily by gastric intubation for 3 weeks (g). # $P < .01$ vs a, b, and e; * $P < .05$ vs. b, ** $P < .01$ vs a; † $P < .001$ vs a and b; § $P < .01$ vs a, b, and e, and § $P < .01$ vs c. (E) Changes in body weight, diet consumption, liver weight, and biological markers in plasma in the same groups as indicated in panel D. * $P < .05$, ** $P < .001$.

frozen sections of the nontumor tissue obtained from the FITC-PLGA-NP-injected STAM mice were incubated with a 1:200 dilution of an Alexa Fluor 647-conjugated rat anti-mouse F4/80 monoclonal antibody (Abcam), fixed with Antifade Mounting Medium with DAPI (Vector Laboratories), and assessed by fluorescence microscopy.

Measurement of ROS Production

In situ ROS production in the liver was assessed by staining with dihydroethidium, as described previously.⁴² Fluorescence intensity was quantified using National Institutes of Health image analysis software for 5 randomly selected areas in the digital images of each mouse.

Cell-Cycle Analysis

Huh7 and HepG2 cells (1×10^5) were cultured in 6-well dishes and incubated with 2DG (0, 1, 10, or 25 mmol/L) for 12 hours. After removing the supernatants and adding Annexin V-FITC and propidium iodide (Annexin V-FLUOS staining kit; Roche Applied Science, Penzberg, Germany), the cell cycle was analyzed using a FACS flow cytometer (FACSCanto II; BD Biosciences, Franklin Lakes, NJ).

Measurement of GSH Production

GSH production was measured using a GSSG/GSH Quantification kit (Dojindo Molecular Laboratories, Kumamoto Japan) according to the manufacturer's instructions. Briefly, Huh7 and HepG2 cells were cultured in 96-well plates at a density of 3×10^3 cells/well, and incubated with 2DG (0, 0.2, 1, or 5 mmol/L) for 24 hours. After adding the GSH assay solution, absorbance of the sample was measured at 405 nm using a FLUO star OPTIMA system (BMG Technologies, Offenburg, Germany).

Assessment of Apoptosis

Apoptotic cells in xenograft tumors were assessed by the terminal deoxynucleotidyl transferase-mediated deoxyuridine triphosphate nick-end labeling method, using an in situ apoptosis detection kit (TaKaRa Bio, Inc, Tokyo, Japan) according to the manufacturer's instructions. Briefly, fragmented DNA was detected histochemically in frozen sections of the xenograft tumors via the in situ incorporation of fluorescein-labeled nucleotides in situ onto the 3' ends of the DNA fragments. Fluorescein-labeled tissues were fixed with Antifade mounting medium with DAPI and assessed by fluorescence microscopy.

Real-Time Reverse-Transcription Polymerase Chain Reaction

Total RNA was extracted from the frozen tumor tissues using the RNeasy mini kit (QIAGEN, Hilden, Germany) and reverse-transcribed into complementary DNA using a Superscript III reverse-transcription kit (Invitrogen, Waltham, MA). mRNA levels were determined using an ABI Prism 7500 sequence detection system (Invitrogen) and cataloged primers (mouse *Cxcl9* Mm00434946_m1, mouse *Cxcl10* Mm00445235_m1, mouse *Cxcl11* Mm00444662_m1, human

IFN- γ Hs00989291_m1, human *CXCL9* Hs00171065_m1, human *CXCL10* Hc00171042_m1, and human *CXCL11* Hc00171138_m1) (Applied Biosystems, Foster City, CA), according to the supplier's recommendations. The mRNA levels of *CXCL9/CXCL10/CXCL11* were measured in the presence or absence of compound C.

Measurement of CXCL9, CXCL10, and CXCL11 Levels

Huh7 and HepG2 cells (3×10^3 for each) were incubated without or with 2DG (0.1, 1, or 10 mmol/L) for 24 hours in 6-well plates, with the addition of IFN- γ and TNF- α for the final 12 hours of the 24-hour experiment. CXCL9, CXCL10, and CXCL11 concentrations in the supernatants of cell cultures were determined using a Quantikine Enzyme-Linked Immunosorbent Assay kit (R&D Systems, Inc, Minneapolis, MN) according to the manufacturer's instructions.

CD8⁺ T-Cell and Treg Isolation

Peripheral blood mononuclear cells from 50 mL of blood collected from healthy human adult volunteers were isolated using Lymphoprep (AXIS-SHIELD, Oslo, Norway) according to the manufacturer's instructions. CD8⁺ T cells and Tregs were isolated from the purified peripheral blood mononuclear cells using a CD8+ T-cell isolation kit (Miltenyi Biotec, Bergisch Gladbach, Germany) and a Treg isolation kit (Miltenyi Biotec), respectively, and suspended in RPMI 1640 containing 1% FBS.

The frequency of the CD8⁺ T cells in these preparations was examined by staining with anti-CD8-FITC and anti-CD3-PE (Tonbo Biosciences, San Diego, CA) using a FACS flow cytometer (FACS Canto II). Likewise, the frequency of Tregs was examined by staining with anti-CD4-FITC, anti-CD25-PE, and anti-CCR4-biotin/streptavidin-APC (Tonbo Biosciences) using a FACS flow cytometer (Aria III; BD Biosciences). We confirmed that these preparations contained more than 90% of CD3⁺/CD8⁺ cells or CD4⁺/CD25⁺/CCR4⁺ cells,⁴³ respectively. The study protocol conformed to the 1975 Helsinki Declaration and was approved by the Institutional Research Ethics Committee (admission no. 3582).

Co-culture of CD8⁺ T Cells and 2DG-PLGA-NP-Treated Huh7 Cells

After the incubation of Huh7 cells (1×10^4) in the presence of 2DG-PLGA-NPs (equivalent to 10 mmol/L 2DG) or PLGA (same weight as 2-DG-PLGA) for 24 hours in 6-well and 96-well plates containing 0 or 900 mg/dL of glucose, lactate production by the Huh7 cells was measured using a glycolysis cell-based assay kit (Cayman Chemical, Ann Arbor, MI) (Figure 6D). Then, CD8⁺ T cells (5×10^4) in cell culture inserts (CC insert MD6 0.4; Thermo Fischer Scientific) were co-cultured with Huh7 cells in 6-well dishes in the presence of 2DG-PLGA-NPs or PLGA for 4 hours, and *IFN- γ* mRNA produced by the CD8⁺ T cells subsequently was measured. Aside from this co-culture, the CD8⁺ T cells in the cell culture inserts were co-cultured with Huh7 cells in 96-well plates for 16 hours after medium exchange and

the addition of 2-NBDG, and subsequently the 2-NBDG content in the CD8⁺ T cells and Huh7 cells, was measured.

Chemotaxis Assay of the CD8⁺ T Cells and Tregs

A suspension of purified CD8⁺ T cells (5×10^4 cells/well) or CD4⁺/CD25⁺ Tregs (1×10^4 cells/well) was exposed to a chemokine concentration gradient in an EZ-TAXIScan device, as described previously.⁴⁴ Chips that were 4 μ m in depth were used for this study. The chemokine concentration gradient that formed from the chemokine injection side to the cell injection side of the microchannel was generated by adding either 10 μ mol/L recombinant CXCL10 (PeproTech, Rocky Hill, NJ) or 0.32 μ mol/L macrophage-derived chemokine (recombinant human CCL22; Tonbo Biosciences). The migration of the CD8⁺ T cells or Tregs in the microchannel was traced with time-lapse intervals using a charge coupled device camera and analyzed using TAXIScan Analyzer 2 software, as previously reported.⁴⁵

To analyze the effect of lactate on CD8⁺ T-cell chemotaxis, CD8⁺ T cells were incubated in culture medium with the pH adjusted to 7.2 by lactate or hydrochloric acid or without pH adjustment for 24 hours. The CD8⁺ T cells in each group were aligned on the cell injection side of the microchannel and assessed for their migration.

To analyze the effect of IFN- γ on CD8⁺ T-cell chemotaxis, CD8⁺ T cells (1×10^4 cells/well) were incubated with IFN- γ (1 μ g/mL) (PeproTech) for 20 hours at 37°C. The culture supernatant was injected into the chemoattractant injection side of the microchannel with or without an anti-CXCR3 neutralizing antibody (Bio X Cell). The CD8⁺ T cells recovered from the co-culture were aligned on the cell injection side, and assessed for their migration without CXCL10 added to the chemoattractant injection side of the microchannel.

To analyze the effect of the IFN- γ - and TNF- α -stimulated Huh7 cells with/without 2DG treatment on CD8⁺ T-cell chemotaxis, the Huh7 cells (1×10^4 cells/well) were incubated with/without 2DG (10 mmol/L) for 24 hours in 6-well plates, with IFN- γ and TNF- α (PeproTech) added and incubated for the final 12 hours of the 24-hour experiment. The Huh7 cells were aligned on the chemoattractant injection side of the microchannel with or without an anti-CXCR3.

To analyze the effect of co-culture of CD8⁺ T cells and 2DG-PLGA-NP-treated Huh7 cells on CD8⁺ T-cell chemotaxis, the CD8⁺ T cells that had been co-cultured with 2DG-PLGA-NP-treated Huh7 cells for 16 hours, as described earlier, were aligned on the cell injection side and assessed for their migration. Similarly, the Tregs that had been co-cultured with the 2DG-PLGA-NP-treated Huh7 cells under the same conditions as the CD8⁺ T cells were assessed for their chemotaxis under an CCL22 concentration gradient.

Finally, to analyze the direct effect of 2DG on CD8⁺ T-cell chemotaxis, CD8⁺ T cells were incubated with 2DG (0, 1, 10, or 50 mmol/L) for 24 hours in the presence or absence of glucose (900 mg/dL), and then assessed for their migration. To obtain statistical data regarding cell migration, the median values of the velocity and directionality of the CD8⁺ T cells or Treg for each experimental period were calculated

from the migratory pathway data obtained from the time-lapse images; the data are expressed in velocity-directionality plots.

Measurement of the Biochemical Markers in Serum

The levels of blood glucose, alanine aminotransferase, total cholesterol, and triglycerides in mouse plasma were determined using a SPOTCHEM EZ SP-4430 system (ARK-RAY, Kyoto, Japan) according to the manufacturer's instructions.

Statistics

Quantitative values are expressed as the means \pm SD. Two groups among the multiple groups were compared using the rank-based, Kruskal-Wallis analysis of variance test, followed by the Tukey test. The data of 2 groups were compared by the Student *t* test for continuous variables. A *P* value less than .05 was considered significant.

References

- White DL, Thrift AP, Kanwal F, Davila J, El-Serag HB. Incidence of hepatocellular carcinoma in all 50 United States, from 2000 through 2012. *Gastroenterology* 2017;152:812–820 e5.
- Cabibbo G, Enea M, Attanasio M, Bruix J, Craxì A, Cammà C. A meta-analysis of survival rates of untreated patients in randomized clinical trials of hepatocellular carcinoma. *Hepatology* 2010; 51:1274–1283.
- Llovet JM, Ricci S, Mazzaferro V, Hilgard P, Gane E, Blanc JF, de Oliveira AC, Santoro A, Raoul JL, Forner A, Schwartz M, Porta C, Zeuzem S, Bolondi L, Greten TF, Galle PR, Seitz JF, Borbath I, Häussinger D, Giannaris T, Shan M, Moscovici M, Voliotis D, Bruix J; SHARP Investigators Study Group. Sorafenib in advanced hepatocellular carcinoma. *N Engl J Med* 2008;359:378–390.
- Kudo M, Finn RS, Qin S, Han KH, Ikeda K, Piscaglia F, Baron A, Park JW, Han G, Jassem J, Blanc JF, Vogel A, Komov D, Jeffrey Evans TR, Lopez C, Dutcus C, Guo M, Saito K, Kraljevic S, Tamai T, Ren M, Cheng AL. Lenvatinib vs. sorafenib in first-line treatment of patients with unresectable hepatocellular carcinoma: a randomized phase 3 non-inferiority trial. *Lancet* 2018; 391:1163–1173.
- Tennant DA, Duran RV, Gottlieb E. Targeting metabolic transformation for cancer therapy. *Nat Rev cancer* 2010;10:267–277.
- Warburg O. Metabolism of tumors. *Biochem Zeitschr* 1923;142:317–333.
- Brand A, Singer K, Koehl GE, Kolitzus M, Schoenhammer G, Thiel A, Matos C, Bruss C, Klobuch S, Peter K, Kastenberger M, Bogdan C,

- Schleicher U, Mackensen A, Ullrich E, Fichtner-Feigl S, Kesselring R, Mack M, Ritter U, Schmid M, Blank C, Dettmer K, Oefner PJ, Hoffmann P, Walenta S, Geissler EK, Pouyssegur J, Villunger A, Steven A, Seliger B, Schreml S, Haferkamp S, Kohl E, Karrer S, Berneburg M, Herr W, Mueller-Klieser W, Renner K, Kreutz M. LDHA-associated lactic acid production blunts tumor immunosurveillance by T and NK cells. *Cell Metab* 2016;24:657–671.
8. Cascone T, McKenzie JA, Mbofung RM, Punt S, Wang Z, Xu C, Williams LJ, Wang Z, Bristow CA, Carugo A, Peoples MD, Li L, Karpinets T, Huang L, Malu S, Creasy C, Leahey SE, Chen J, Chen Y, Pelicano H, Bernatchez C, Vashisht Gopal YN, Heffernan TP, Hu J, Wang J, Amaria RN, Garraway LA, Huang P, Yang P, Wistuba II, Woodman SE, Roszik J, Davis RE, Davies MA, Heymach JV, Hwu P, Peng W. Increased tumor glycolysis characterizes immune resistance to adaptive T cells therapy. *Cell Metab* 2018;27:977–987.
 9. Zhu AX, Finn RS, Edeline J, Cattani S, Ogasawara S, Palmer D, Verslype C, Zagonel V, Fartoux L, Vogel A, Sarker D, Verset G, Chan SL, Knox J, Daniele B, Webber AL, Ebbinghaus SW, Ma J, Siegel AB, Cheng AL, Kudo M; KEYNOTE-224 Investigators. Pembrolizumab in patients with advanced hepatocellular carcinoma previously treated with sorafenib (KEYNOTE-224): a non-randomised, open-label phase 2 trial. *Lancet Oncol* 2018;19:940–952.
 10. Finn RS, Qin S, Ikeda M, Galle PR, Ducreux M, Kim TY, Kudo M, Breder V, Merle P, Kaseb AO, Li D, Verret W, Xu DZ, Hernandez S, Liu J, Huang C, Mulla S, Wang Y, Lim HY, Zhu AX, Cheng AL; for the IMbrave 150 Investigators. Atezolizumab plus bevacizumab in unresectable hepatocellular carcinoma. *N Engl J Med* 2020;382:1894–1905.
 11. Raez LE, Papadopoulos K, Ricart AD, Chiorean EG, Dipaola RS, Stein MN, Rocha Lima CM, Schlesselman JJ, Tolba K, Langmuir VK, Kroll S, Jung DT, Kurtoglu M, Rosenblatt J, Lampidis TJ. A phase I dose-escalation trial of 2-deoxy-D-glucose alone or combined with docetaxel in patients with advanced solid tumors. *Cancer Chemother Pharmacol* 2013;71:523–530.
 12. Stein M, Lin H, Jeyamohan C, Dvorzhinski D, Gounder M, Bray K, Eddy S, Goodin S, White E, Dipaola RS. Targeting tumor metabolism with 2-deoxyglucose in patients with castrate-resistant prostate cancer and advanced malignancies. *Prostate* 2010;70:1388–1394.
 13. Goel S, Duda DG, Xu L, Munn LL, Boucher Y, Fukumura D, Jain RK. Normalization of the vascular for treatment of cancer and other disease. *Physiol Rev* 2011;91:1071–1121.
 14. Matsumura Y, Maeda H. A new concept for macromolecular therapeutics in cancer chemotherapy: mechanism of tumorotropic accumulation of proteins and the antitumor agent smancs. *Cancer Res* 1986;46:6387–6392.
 15. Maeda H, Tsukigawa K, Fang J. A retrospective 30 years after discovery of the enhanced permeability and retention effect of solid tumors: next-generation chemotherapeutics and photodynamic therapy—problems, solutions, and prospects. *Microcirculation* 2016;23:173–182.
 16. Nichols JW, Bae YH. EPR: evidence and fallacy. *J Control Release* 2014;190:451–464.
 17. Danhier F, Ansorena E, Silva JM, Coco R, Breton AL, Préat V. PLGA-based nanoparticles: an overview of biomedical applications. *J Control Release* 2012;161:505–522.
 18. Park JH, Cho HJ, Kim DD. Poly((D,L)lactic-glycolic) acid-star glucose nanoparticles for glucose transporter and hypoglycemia-mediated tumor targeting. *Int J Nanomedicine* 2017;12:7453–7467.
 19. Xing J, Bhuria V, Bui KC, Nguyen MLT, Hu Z, Hsieh CJ, Wittstein K, Stadler M, Wilkens L, Li J, Kalesse M, Bozko P, Plentz RR. Haprolid inhibits tumor growth of hepatocellular carcinoma through Rb/E2F and Akt/mTOR inhibition. *Cancers* 2020;12:e615.
 20. Ou JM, Qui MK, Dai YX, Dong Q, Shen J, Dong P, Wang XF, Liu YB, Fei ZW. Combined blockade of Akt/mTOR pathway inhibits growth of human hemangioma via downregulation of proliferating cell nuclear antigen. *Int J Immunopathol Pharmacol* 2012;25:945–953.
 21. Averous J, Fonseca BD, Proud CG. Regulation of cyclin D1 expression by mTORC1 signaling requires eukaryotic initiation factor 4E-binding protein 1. *Oncogene* 2008;27:1106–1113.
 22. Wang S, Lu J, You Q, Huang H, Chen Y, Liu K. The mTOR/AP-1/VEGF signaling pathway regulates vascular endothelial cell growth. *Oncotarget* 2016;7:53269–53276.
 23. Zhang D, Li J, Wang F, Hu J, Wang S, Sun Y. 2-Deoxy-D-glucose targeting of glucose metabolism in cancer cells as a potential therapy. *Cancer Lett* 2014;355:176–183.
 24. Tokunaga R, Zhang W, Naseem M, Puccini A, Berger MD, Soni S, McSkane M, Baba H, Lenz HJ. CXCL9, CXCL10, CXCL11/CXCR3 axis for immune activation—a target for novel cancer therapy. *Cancer Treat Rev* 2018;63:40–47.
 25. Rauch I, Müller M, Decker T. The regulation of inflammation by interferons and their STATs. *JAK-STAT* 2013;2:e23820.
 26. Peng D, Kryczek I, Nagarsheth N, Zhao L, Wei S, Wang W, Sun Y, Zhao E, Vatan L, Szeliga W, Kotarski J, Tarkowski R, Dou Y, Cho K, Hensley-Alford S, Munkarah A, Liu R, Zou W. Epigenetic silencing of Th1 type chemokines shapes tumor immunity and immunotherapy. *Nature* 2015;527:249–253.

27. Wan L, Xu K, Wei Y, Zhang J, Han T, Fry C, Zhang Z, Wang YV, Huang L, Yuan M, Xia W, Chang WC, Huang WC, Liu CL, Chang YC, Liu J, Wu Y, Jin VX, Dai X, Guo J, Liu J, Jiang S, Li J, Asara JM, Brown M, Hung MC, Wei W. Phosphorylation of EZH2 by AMPK suppresses PRC2 methyltransferase activity and oncogenic function. *Mol Cell* 2018;69:279–291.
28. Groom JR, Luster AD. CXCR3 in T cell function. *Exp Cell Res* 2011;317:620–631.
29. Bhat P, Leggatt G, Waterhouse N, Frazer IH. Interferon- γ derived from cytotoxic lymphocytes directly enhances their motility and cytotoxicity. *Cell Death Dis* 2017;8:e2836.
30. Mailloux AW, Young MRI. NK-dependent increases in CCL22 secretion selectively recruits regulatory T cells to the tumor microenvironment. *J Immunol* 2009;182:2753–2765.
31. Poisson J, Lemoinne S, Boulanger C, Durand F, Moreau R, Valla D, Rautou PE. Liver sinusoidal endothelial cells: physiology and role in liver diseases. *J Hepatol* 2017;66:212–227.
32. Von Schulthess G, Steinert HC, Hany TF. Integrated PET/CT: current applications and future directions. *Radiology* 2006;238:405–422.
33. Lee JH, Park JY, Kim DY, Ahn SH, Han KH, Seo HJ, Lee JD, Choi HJ. Prognostic value of 18F-FDG PET for hepatocellular carcinoma patients treated with sorafenib. *Liver Int* 2011;31:1144–1149.
34. Sica A, Dorman L, Viggiano V, Cippitelli M, Ghosh P, Rice N, Young HA. Interaction of NF-kappaB and NFAT with the interferon-gamma promoter. *J Biol Chem* 1997;272:30412–30420.
35. Cham CM, Driessens G, O’Keefe JP, Gajewski TF. Glucose deprivation inhibits multiple key gene expression events and effector functions in CD8⁺T cells. *Eur J Immunol* 2008;38:2438–2450.
36. Chang CH, Curtis JD, Maggi LB, Faubert B, Villarino AV, O’Sullivan D, Huang SC, van der Windt GJ, Blagih J, Qiu J, Weber JD, Pearce EJ, Jones RG, Pearce EL. Posttranscriptional control of T cell effector function by aerobic glycolysis. *Cell* 2013;153:1239–1251.
37. Chang CH, Qiu J, O’Sullivan D, Buck MD, Noguchi T, Curtis JD, Chen Q, Gindin M, Gubin MM, van der Windt GJ, Tonc E, Schreiber RD, Pearce EJ, Pearce EL. Metabolic competition in the tumor microenvironment is a driver of cancer progression. *Cell* 2015;162:1229–1241.
38. Landau BR, Laszlo J, Stengle J, Burk D. Certain metabolic and pharmacological effects in cancer patients given infusions of 2-deoxy-D-glucose. *J Natl Cancer Inst* 1958;21:485–494.
39. Chen L, Nakano K, Kimura S, Matoba T, Iwata E, Miyagawa M, Tsujimoto H, Nagaoka K, Kishimoto J, Sunagawa K, Egashira K. Nanoparticle-mediated delivery of pitavastatin into lungs ameliorates the development and induces regression of monocrotaline-induced pulmonary artery hypertension. *Hypertension* 2011;57:343–350.
40. Barreira da Silva R, Laird ME, Yatim N, Fiette L, Ingersoll MA, Albert ML. Dipeptidylpeptidase 4 inhibition enhances lymphocyte trafficking, improving both naturally occurring tumor immunity and immunotherapy. *Nat Immunol* 2015;16:850–858.
41. Nishina S, Yamauchi A, Kawaguchi T, Kaku K, Goto M, Sasaki K, Hara Y, Tomiyama Y, Kuribayashi F, Torimura T, Hino K. Dipeptidyl peptidase 4 inhibitors reduce hepatocellular carcinoma by activating lymphocyte chemotaxis in mice. *Cell Mol Gastroenterol Hepatol* 2019;7:115–134.
42. Nishina S, Hino K, Korenaga M, Vecchi C, Pietrangelo A, Mizukami Y, Furutani T, Sakai A, Okuda M, Hidaka I, Okita K, Sakaida I. Hepatitis C virus-induced reactive oxygen species raise hepatic iron level in mice by reducing hepcidin transcription. *Gastroenterology* 2008;134:226–238.
43. Viguier M, Lemaitre F, Verola O, Cho MS, Gorochov G, Dubertret L, Bachelez H, Kourilsky P, Ferradini L. Foxp3 expressing CD4⁺/CD25^{high} regulatory T cells are overrepresented in human metastatic melanoma lymph nodes and inhibit the function of infiltrating T cells. *J Immunol* 2004;173:1444–1453.
44. Kanegasaki S, Nomura Y, Nitta N, Akiyama S, Tamatani T, Goshoh Y, Yoshida T, Sato T, Kikuchi Y. A novel optic assay for the quantitative measurement of chemotaxis. *J Immunol Methods* 2003;282:1–11.
45. Yamauchi A, Degawa-Yamauchi M, Kuribayashi F, Kanegasaki S, Tsuchiya T. Systematic single cell analysis of migration and morphological changes of human neutrophils over stimulus concentration gradients. *J Immunol Methods* 2014:404–459, 70.

Received July 3, 2020. Accepted October 19, 2020.

Correspondence

Address correspondence to: Keisuke Hino, MD, PhD, or Sohji Nishina, MD, PhD, Kawasaki Medical School, Kurashiki, Okayama, 701-0192 Japan. e-mail: f018ep@med.kawasaki-m.ac.jp; khino@med.kawasaki-m.ac.jp; fax: (81) 864641196.

Acknowledgments

The authors thank Fumiaki Takenaka, Okayama University, for supporting the experimental facilities (in vivo imaging system) essential for the completion of the work. The authors also thank Ms Mizukawa, Ms Nagato, and Ms Fujioka for their technical assistance for the experiments. The authors thank Springer Nature Author Services for providing writing assistance.

Conflicts of interest

The authors disclose no conflicts.

Funding

Supported by a Grant-in Aid for Scientific Research (B) (19H03644) from the Japan Society for the Promotion of Science (K.H.), by a Grant-in Aid for Scientific Research (C) (18K07923 to S.N.), and by a Grant-in Aid for Scientific Research (C) (19K07676 to A.Y.).